


Oscillatory pressure-driven rarefied binary gas mixture flow between parallel plates

Alexandros Tsimpoukis¹,* Stergios Naris¹, and Dimitris Valougeorgis¹
Department of Mechanical Engineering, University of Thessaly, 38334 Volos, Greece

 (Received 20 November 2020; accepted 22 February 2021; published 15 March 2021)

The rarefied, oscillatory, pressure-driven binary gas mixture flow between parallel plates is computationally investigated in terms of the mixture molar fraction and molecular mass ratio of the species, in a wide range of gas rarefaction and oscillation frequency. Modeling is based on the McCormack kinetic model. The output quantities are in dimensionless form and include the flow rate, wall shear stress and pumping power of the mixture, as well as the velocity and shear stress distributions and flow rates of the species. The presented results are for He-Xe and Ne-Ar. The heavier species are affected more drastically than the lighter ones from the inertial forces, resulting to large differences between the flow rate amplitudes of the species, which are increased as the flow becomes less rarefied, provided that the oscillation frequency is adequately high. At very high frequencies the ratio of the flow rate amplitudes of the light over the heavy species tends to the inverse of their molecular mass ratio in the whole range of gas rarefaction. The velocity overshooting effect becomes more pronounced as the molecular mass is increased. The mixture flow rate amplitude is larger, while its phase angle is smaller, than the corresponding ones of single gas, and they both vary nonmonotonically with the molar fraction. The effect of the mixture composition on the wall shear stress and pumping power is small. The present work may be useful in the design of gas separation devices, operating at moderate and high frequencies in rarefied and dense atmospheres.

DOI: [10.1103/PhysRevE.103.033103](https://doi.org/10.1103/PhysRevE.103.033103)

I. INTRODUCTION

Oscillatory flows in the hydrodynamic regime are very common. They are driven by moving boundaries [1] or pressure gradients [2,3], oscillating harmonically in time with some specified frequency. Similarly, rarefied oscillatory flows are encountered in enclosures, driven by moving boundaries, oscillating parallel or vertical to the main flow [4–8], and in capillaries of various cross sections, driven by oscillating or pulsatile pressure or force gradients [9–11]. Since in rarefied gas flows the classical Navier-Stokes-Fourier approach is not applicable, kinetic modeling and simulations, based on the computational solution of the Boltzmann equation or of reliable kinetic model equations via deterministic [12] or stochastic schemes [13], must be implemented. It is noted that oscillatory gas flows are in the so-called hydrodynamic (or viscous) regime, when both the mean free path and collision frequency are much smaller than the characteristic length and oscillation frequency respectively. When either of these restrictions is relaxed, the flow is classified as rarefied and may be in the so-called transition or free molecular regimes depending on the time and space characteristic scales [5,6,9,10].

Rarefied boundary-driven oscillatory flows of single gases have been extensively investigated over the last two decades [4–8,14–20]. These flows are present in a variety of systems, such as resonating filters, sensors and actuators, where the computation of the damping forces is crucial in order to control and optimize the resolution and sensitivity of the

signal [21]. Combined effects of harmonically oscillating both the boundary velocity and temperature, have been also considered to enhance the acoustic transduction or even to achieve acoustic cloaking [20,22]. Very recently, propagation of sound waves due to mechanical and thermal excitation through binary gas mixtures has been also considered [23–28]. The investigated setups include flow configurations in half-space, slab, rectangular cavities, comb-drives, and nonplanar geometries, and the implemented numerical schemes are mainly based on the stochastic Direct Simulation Monte Carlo (DSMC) method [4,14,19,20,22] and the deterministic solution of kinetic model equations by the discrete velocity method [5,6,26,27]. The latter approach is introduced when the amplitude of the oscillatory velocity and/or temperature driving the flow is small by applying the linearized Bhatnagar-Gross-Krook (BGK) model [29] in single gas flows and the McCormack model [30] in binary gas mixture flows.

On the contrary, rarefied pressure-driven oscillatory or pulsatile gas flows have attracted much less attention. The reported investigations refer to fully developed single gas flows in capillaries [9–11,31], with applications in vapor deposition [32], cryogenic pulse tubes [33] and microfluidic oscillators and pumps [34–37]. However, it is important to note that in the hydrodynamic regime pressure-driven oscillatory or pulsatile gas flows are encountered in numerous technological fields, such as pneumatic lines and control systems [38], reciprocating pumps [39], internal or external manifolds of combustion engines [40], and bio-engineering [41]. They are also encountered in mass and heat transfer processes, where many investigations have been performed to enhance, gas separation or mixing, species

*atsimpoukis@mie.uth.gr

contaminants dispersion and thermal diffusion [42–47]. Therefore, taking into consideration that oscillatory pressure-driven gas flows in the hydrodynamic regime are very common, along with the progress in fabrication techniques of micro devices (sensors/actuators, pumps/compressors, cooling systems, piping manifolds, separators), it is reasonable to expect that oscillatory pressure-driven rarefied flows of single gases and gas mixtures have significant technological potential and should be theoretically investigated.

Recently, rarefied, pressure-driven, oscillatory, fully developed single gas flows through tubes and rectangular ducts have been investigated [9–11]. It has been found that various interesting effects (e.g., velocity overshooting, phase angle lag between velocity and pressure gradient, etc.), well known in corresponding viscous oscillatory flows [3], are still present but higher oscillation frequencies are needed to trigger these phenomena. No corresponding work for oscillatory gas mixture flows is available. Of course stationary binary and ternary gas mixtures flows through capillaries of various cross sections in the whole range of the Knudsen number have been extensively investigated [48–53]. These flows have strong theoretical interest because, compared to the ones with single gases, new nonequilibrium phenomena occur. One of these phenomena is the so-called gas separation phenomenon, which is contributed to the different molecular speeds of the component of the gas mixture [54–57]. Gas separation is almost always present in rarefied gas mixture flows and depending upon the application it should be either enlarged or reduced. Therefore, recently there has been substantial effort in the design of devices controlling gas separation and/or mixing. Some designs, based on the Knudsen pump operating principal, have been materialized [58–60], while others are in a preliminary conceptual stage [61–65].

In this context, the present work is devoted in the detailed theoretical investigation of the rarefied oscillatory fully developed binary gas mixture flow between parallel plates due to harmonically oscillating pressure gradient, imposed parallel to the plates. The mixture consists of monatomic gases. Modeling is based on the time-dependent linearized McCormack kinetic model equation subject to diffuse boundary conditions via the discrete velocity method. The investigation is focused on the effect of the molecular mass ratio of the components of the mixture and of its molar fraction on the oscillatory behavior of the velocity distribution, flow rate, shear stress, and pumping power of the species and the mixture, in a wide range of the gas rarefaction and oscillation frequency. Attention is also given to the effect of the oscillation frequency on gas separation. The objective of the work is to provide for various representative binary gas mixtures a complete and detailed view of the flow characteristics of the light and heavy species and of the mixture in the whole range of the molar fraction, gas rarefaction and oscillation frequency. In parallel, all involved flow phenomena are revealed and physically explained.

The remaining of the paper is structured as follows: In Sec. II the flow configuration is described and all input and output quantities, including the dimensionless parameters characterizing the flow, are prescribed. In Sec. III the kinetic formulation and the implemented numerical scheme are presented. The results are presented and discussed in Sec. IV,

which is divided for clarity purposes into three subsections. The concluding remarks are outlined in Sec. V.

II. FLOW CONFIGURATION

Consider the rarefied oscillatory pressure-driven fully developed isothermal binary gas mixture flow between two infinite long parallel plates. The flow is in the x' direction parallel to the plates, which are fixed at $y' = \pm H/2$. The flow is caused by an externally imposed harmonically oscillating pressure gradient of the form

$$\frac{d\tilde{P}}{dx'} = \Re \left[\frac{dP^{(A)}}{dx'} \exp(-i\omega t') \right], \quad (1)$$

where \Re denotes the real part of a complex expression, $P^{(A)}(x')$ and $dP^{(A)}/dx'$ are the amplitudes of the oscillating pressure and pressure gradient, respectively, $i = \sqrt{-1}$, t' is the time-independent variable, and ω is the oscillation (cyclic) frequency. Throughout the paper, quantities with tilde are real, time-dependent quantities. In the hydrodynamic regime, this flow configuration is a classical one and it is well described in several mechanics textbooks [3,66], while corresponding work in the transition and free molecular regimes is limited only to single gases [9,10]. Furthermore, the assumption that the fluid oscillates in bulk or en masse [3], i.e., that all quantities oscillate with the same frequency as the pressure gradient, which is well established in oscillatory flows in rigid channels, is also applied in the present work.

The binary gas mixture consists of two monatomic species of molecular masses m_α , with the index “ $\alpha = 1, 2$,” always referring, without loss of generality, to the light and heavy species of the mixture, respectively. The number densities \tilde{n}_α of the species and the number density of the mixture \tilde{n} are related to the corresponding partial pressures \tilde{P}_α and total mixture pressure $\tilde{P} = \tilde{P}_1 + \tilde{P}_2$ with the equation of states as $\tilde{P}_\alpha = \tilde{n}_\alpha kT$ and $\tilde{P} = \tilde{n}kT$, where T is the reference temperature, remaining constant in the flow field, and k is the Boltzmann constant. The mass densities of the species and the mixture are defined as $\tilde{\rho}_\alpha = m_\alpha \tilde{n}_\alpha$ and $\tilde{\rho} = m\tilde{n}$, respectively.

The mixture pressure $\tilde{P}_\alpha(x', t') = \Re[P_\alpha^{(A)}(x') \exp(-i\omega t')]$ oscillates harmonically in time t' with some frequency ω and varies, as in steady-state fully developed flow, linearly with x' . The same applies for the number density of the mixture \tilde{n} , as well as the partial pressures \tilde{P}_α and number densities \tilde{n}_α of the species. Following common practice and without loss of generality, the whole formulation is applied at some arbitrary fixed position x' along the plates. Therefore, in order to simplify notation the x' independent variable is not shown in the macroscopic quantities.

The local number densities of the mixture components oscillate harmonically as

$$\tilde{n}_\alpha(t') = \Re[n_\alpha^{(A)} \exp(-i\omega t')], \quad (2)$$

where $n_\alpha^{(A)}$, $\alpha = 1, 2$, is the local amplitude of the oscillating number density of each species, while the local number density of the mixture is $\tilde{n}(t') = \tilde{n}_1(t') + \tilde{n}_2(t')$. The molar fraction of the mixture is defined as the ratio of the number density of the light species over the mixture number density,

given by

$$\tilde{C}(t') = \Re[C^{(A)} \exp(-i\omega t')], \quad (3)$$

with

$$C^{(A)} = \frac{n_1^{(A)}}{n^{(A)}} = \frac{n_1^{(A)}}{n_1^{(A)} + n_2^{(A)}} \quad (4)$$

being the local amplitude of the molar fraction. Since $C^{(A)}$ is repeatedly used in the paper to simplify notation, the superscript (A) is dropped and $C^{(A)} = C$, while the molar fraction amplitude of the heavy species is $1 - C$. The mean molecular mass of the mixture is given by $m = Cm_1 + (1 - C)m_2$.

Then, the deduced time-dependent local flow quantities of practical interest include the bulk velocity $\tilde{U}_\alpha(t', y')$, shear stress $\tilde{\Pi}_\alpha(t', y')$, and heat flow $\tilde{Q}_\alpha(t', y')$ of the two species $\alpha = 1, 2$, which depend on y' , the space-independent variable vertical to the plates and vary harmonically with time t' . They may be written as

$$\tilde{Z}_\alpha(t, y) = \Re[Z_\alpha(y) \exp(-i\omega t')], \quad (5)$$

where $\tilde{Z}_\alpha(t, y) = [\tilde{U}_\alpha(t, y), \tilde{\Pi}_\alpha(t, y), \tilde{Q}_\alpha(t, y)]$, while $Z_\alpha(y) = [U_\alpha(y), \Pi_\alpha(y), Q_\alpha(y)]$ is a vector of the corresponding complex functions. By combining $U_\alpha(y)$ and $\Pi_\alpha(y)$ the hydrodynamic velocity and shear stress of the gas mixture are obtained as

$$\begin{aligned} U(y) &= \frac{1}{\rho^{(A)}} [\rho_1^{(A)} U_1(y) + \rho_2^{(A)} U_2(y)] \\ &= \frac{m_1}{m} C U_1(y) + \frac{m_2}{m} (1 - C) U_2(y) \end{aligned} \quad (6)$$

and

$$\begin{aligned} \Pi(y) &= \frac{1}{n^{(A)}} [n_1^{(A)} \Pi_1(y) + n_2^{(A)} \Pi_2(y)] \\ &= C \Pi_1(y) + (1 - C) \Pi_2(y), \end{aligned} \quad (7)$$

respectively. In Eq. (6), $\rho_\alpha^{(A)} = m_\alpha n_\alpha^{(A)}$, $\alpha = 1, 2$ and $\rho^{(A)} = mn^{(A)}$ are the amplitudes of the oscillating mass densities of the species and the mixture, respectively. The shear stress at the wall is denoted by Π_W .

In addition, of major theoretical and technological importance are the deduced oscillatory particle flow rates of the two species

$$\tilde{J}_\alpha(t') = \Re[J_\alpha \exp(-i\omega t')], \quad (8)$$

where J_α are complex functions, given by

$$J_\alpha = n_\alpha^{(A)} \int_{-H/2}^{H/2} U_\alpha dy'. \quad (9)$$

The mixture particle flow rate is $\tilde{J} = \tilde{J}_1 + \tilde{J}_2$, with $J = J_1 + J_2$. As is well known in rarefied gas mixture flows, gas separation may occur due to the different molecular speeds of the species [54,55]. In steady-state binary gas flows through capillaries, gas separation is characterized by the ratio of the flow rate of the light over the heavy species, and as this ratio is increased, gas separation is also increased [57]. Similarly, in oscillatory binary gas mixture flows, gas separation may be quantified by the amplitude and the phase angle of the ratio of

the complex flow rates of the species

$$\frac{J_1}{J_2} = \frac{J_1^{(A)}}{J_2^{(A)}} \exp[i(J_1^{(P)} - J_2^{(P)})], \quad (10)$$

where the superscripts (A) and (P) refer to the amplitude and phase angle, respectively, of the flow rates. Obviously as the amplitude ratio and/or the phase angle lag are increased, gas separation is enhanced.

Another overall quantity of practical interest is the pumping power needed to drive the oscillatory mixture flow. More specifically, the pumping power to drive a unit depth fluid element $H \times dx'$ is given by the product of the net pressure force $d\tilde{P} \times H$, acting on the cross section H of the element, times the average hydrodynamic velocity of the mixture $\tilde{U}'(t')$, written as [3,9]

$$\begin{aligned} \tilde{E}'(t') &= Hd\tilde{P}(t')\tilde{U}'(t') \\ &= HdP^{(A)} \cos(\omega t') \Re[\tilde{U} \exp(-i\omega t')], \end{aligned} \quad (11)$$

where $\tilde{U}' = \int_{-H/2}^{H/2} U dy'$. The particle flow rates and the pumping power are given in particles per second per meter and in watts per meter, respectively.

Furthermore, the inertia (or acceleration), viscous and pressure forces of the mixture acting on a fluid volume per unit length (Hdx') are given by

$$\tilde{F}_I(t') = Hdx' \rho^{(A)} \frac{\partial \tilde{U}'(t')}{\partial t'}, \quad (12)$$

$$\tilde{F}_V(t') = 2dx' \tilde{\Pi}_W(t'), \quad (13)$$

and

$$\tilde{F}_P(t') = Hd\tilde{P}(t'), \quad (14)$$

respectively, $\tilde{U}'(t')$ is the average hydrodynamic velocity of the mixture and $\tilde{\Pi}_W(t')$ is the wall shear stress of the mixture. At any time over a cycle, since there is no net momentum flux, the net sum of the inertia and viscous forces, which may add or subtract to each other at different times within the oscillatory cycle, must be equal to the pressure force driving the oscillatory flow, i.e., $\tilde{F}_P(t') = \tilde{F}_I(t') + \tilde{F}_V(t')$.

At this stage it is convenient to introduce the dimensionless independent variables

$$x = x'/H, \quad y = y'/H, \quad t = t'\omega, \quad (15)$$

the dimensionless amplitude of the local pressure gradient

$$X_P = \frac{H}{P^{(A)}} \frac{dP^{(A)}}{dx'} = \frac{1}{P^{(A)}} \frac{dP^{(A)}}{dx} \ll 1, \quad (16)$$

and the characteristic speed of the mixture $v = \sqrt{2kT/m}$. The condition of $X_P \ll 1$ is due to the fully developed flow assumption. Then, the bulk velocity, shear stress, and heat flow in Eq. (5) are nondimensionalized by (vX_P) , $(2P^{(A)}X_P)$, and $(vP^{(A)}X_P)$, respectively, to yield the following:

$$\begin{aligned} \tilde{u}_\alpha(t, y) &= \Re[u_\alpha(y) \exp(-it)] \\ &= \Re[u_\alpha^{(A)}(y) \exp\{i[u_\alpha^{(P)}(y) - t]\}] \\ &= u_\alpha^{(A)}(y) \cos[t - u_\alpha^{(P)}(y)], \end{aligned} \quad (17)$$

$$\begin{aligned}\tilde{\omega}_\alpha(t, y) &= \mathbb{R}[\varpi_\alpha(y) \exp(-it)] \\ &= \mathbb{R}[\varpi_\alpha^{(A)}(y) \exp\{i[\varpi_\alpha^{(P)}(y) - t]\}] \\ &= \varpi_\alpha^{(A)}(y) \cos[t - \varpi_\alpha^{(P)}(y)],\end{aligned}\quad (18)$$

$$\begin{aligned}\tilde{q}_\alpha(t, y) &= \mathbb{R}[q_\alpha(y) \exp(-it)] \\ &= \mathbb{R}[q_\alpha^{(A)}(y) \exp\{i[q_\alpha^{(P)}(y) - t]\}] \\ &= q_\alpha^{(A)}(y) \cos[t - q_\alpha^{(P)}(y)].\end{aligned}\quad (19)$$

The superscripts (A) and (P) always refer to the real-valued distributions of the amplitude and the phase angle respectively of each complex quantity. Obviously, the dimensionless time-dependent bulk velocity $\tilde{u}_\alpha(t, y)$, shear stress $\tilde{\omega}_\alpha(t, y)$ and heat flow $\tilde{q}_\alpha(t, y)$ of the two species are not necessarily in phase to each other and more importantly to the oscillating pressure gradient in Eq. (1). The dimensionless velocity and shear stress of the mixture [see Eqs. (6) and (7)] are denoted by $u(y)$ and $\varpi(y)$, respectively.

Furthermore, the flow rates in Eqs. (8) and (9) are nondimensionalized by $(P^{(A)}X_P H/mv)$ to obtain the dimensionless oscillatory particle flow rates of each species

$$\begin{aligned}\tilde{G}_\alpha(t') &= \mathbb{R}[G_\alpha \exp(-it)] = \mathbb{R}[G_\alpha^{(A)} \exp\{i(G_\alpha^{(P)} - t)\}] \\ &= G_\alpha^{(A)} \cos[t - G_\alpha^{(P)}],\end{aligned}\quad (20)$$

where

$$G_\alpha = G_\alpha^{(A)} \exp(iG_\alpha^{(P)}) = 2 \int_{-1/2}^{1/2} u_\alpha dy. \quad (21)$$

Also, it is readily deduced that the ratio J_1/J_2 , defined in Eq. (10), is rewritten as

$$\frac{J_1}{J_2} = \frac{C}{1-C} \frac{G_1}{G_2}, \quad (22)$$

or in the more convenient form

$$\frac{J_1}{J_2} \frac{1-C}{C} = \frac{G_1}{G_2} = \frac{G_1^{(A)}}{G_2^{(A)}} \exp[i(G_1^{(P)} - G_2^{(P)})]. \quad (23)$$

Thus, the ratio $G_1/G_2 = (J_1/J_2)[(1-C)/C]$ is equivalent to the so-called separation parameter in [57] and fully characterizes the gas separation intensity, which is specified by computing the amplitude ratio $G_1^{(A)}/G_2^{(A)}$ and the phase angle difference $G_1^{(P)} - G_2^{(P)}$. Furthermore, the dimensionless oscillatory particle flow rate of the mixture is given by

$$\begin{aligned}\tilde{G}(t) &= \mathbb{R}[G \exp(-it)] = \mathbb{R}[G^{(A)} \exp\{i(G^{(P)} - t)\}] \\ &= G^{(A)} \cos[t - G^{(P)}],\end{aligned}\quad (24)$$

where

$$G = CG_1 + (1-C)G_2. \quad (25)$$

The pumping power in Eq. (11) is nondimensionalized by $(vX_P)(X_P H P^{(A)})$ to find the dimensionless oscillatory pumping power

$$\begin{aligned}\tilde{E}(t) &= dx \cos(t) \mathbb{R}[\tilde{u} \exp(-it)] \\ &= \frac{1}{2} dx \cos(t) \mathbb{R}\left[\left[\frac{m_1}{m} CG_1 + \frac{m_2}{m} (1-C)G_2\right] \exp(-it)\right],\end{aligned}\quad (26)$$

needed to drive the dimensionless fluid element ($1 \times dx$), with $dx = dx'/H$. Here, the dimensionless mean velocity has been substituted by the dimensionless flow rate, since it is readily seen that $G_\alpha = 2\tilde{u}_\alpha$. By integrating Eq. (26) over one oscillation cycle, the average pumping power over the cycle is derived as

$$\begin{aligned}\bar{E} &= \frac{1}{2\pi} \int_0^{2\pi} \tilde{E}(t) dt \\ &= \frac{1}{4} dx \left[\frac{m_1}{m} CG_1^{(A)} \cos G_1^{(P)} + \frac{m_2}{m} (1-C)G_2^{(A)} \cos G_2^{(P)} \right].\end{aligned}\quad (27)$$

It is pointed out that although the net flow rate over one cycle is zero, a nonzero cycle-average pumping power is required to maintain the oscillatory flow. In the low-frequency regime, where the imaginary part of all macroscopic quantities is gradually diminished and the phase angles tend to zero, the steady-state solution is approached. In addition, the inertia, viscous and pressure forces are all divided by $(HP^{(A)}X_P)$ to yield the corresponding dimensionless ones:

$$\begin{aligned}\tilde{f}_I(t') &= 2dx \frac{\delta}{\theta} \frac{\partial \tilde{u}'(t')}{\partial t} \\ &= dx \frac{\delta}{\theta} \left[\frac{m_1}{m} CG_1^{(A)} \sin(G_1^{(P)} - t) \right. \\ &\quad \left. + \frac{m_2}{m} (1-C)G_2^{(A)} \sin(G_2^{(P)} - t) \right],\end{aligned}\quad (28)$$

$$\tilde{f}_V(t') = 4dx \tilde{\omega}_W(t') = 4dx \varpi_W^{(A)} \cos(t - \varpi_W^{(P)}), \quad (29)$$

$$\tilde{f}_P(t') = dx \cos t. \quad (30)$$

The force balance expression in dimensionless form reads as

$$\tilde{f}_P(t) = \tilde{f}_I(t) + \tilde{f}_V(t), \quad (31)$$

and substituting Eqs. (28)–(30) into Eq. (31) yields the force balance expression in dimensionless form:

$$\begin{aligned}\frac{\delta}{\theta} \left[\frac{m_1}{m} CG_1^{(A)} \sin(G_1^{(P)} - t) + \frac{m_2}{m} (1-C)G_2^{(A)} \sin(G_2^{(P)} - t) \right] \\ + 4\varpi_W^{(A)} \cos(t - \varpi_W^{(P)}) \\ = \cos t.\end{aligned}\quad (32)$$

The time-dependent force balance expression (32) is used for confirming the accuracy of the computed amplitudes and angle phases of the flow rate and the shear stress.

The objectives of the present work include the computation of the macroscopic distributions of the velocity and shear stress in Eqs. (17) and (18), the particle flow rates of the species and the mixture in Eqs. (20)–(25), and the pumping powers in Eqs. (26) and (27), in terms of the parameters characterizing the flow. As in the case of oscillatory single gas flow, the oscillatory binary gas mixture flow between parallel plates is also characterized by the gas rarefaction and oscillation parameters [5,6,10]. The gas rarefaction parameter is proportional to the inverse Knudsen number, defined as

$$\delta = \frac{P^{(A)}H}{v\mu}, \quad (33)$$

where H is the distance between the plates, v is the characteristic speed of the mixture, and μ is the viscosity coefficient of the mixture at reference temperature T . The oscillation parameter is the ratio of the intermolecular collision frequency defined as $\nu = P^{(A)}/\mu$ over the oscillation frequency ω , given by

$$\theta = \frac{P^{(A)}}{\mu\omega}. \quad (34)$$

The flow is in the hydrodynamic regime when both $\delta \gg 1$ and $\theta \gg 1$ [12]. The steady-state conditions are reached as $\theta \rightarrow \infty$ ($\omega \rightarrow 0$). In addition to δ and θ , the composition of the binary gas mixture, i.e., the molecular masses m_1 and m_2 of the two monatomic components, as well as the amplitude of the molar fraction C , must be specified.

Once the parameters δ , θ , m_1 , m_2 , and C are defined, the input data are complete, and the flow behavior and characteristics for any binary gas mixture in the whole range of the gas rarefaction and oscillation frequencies may be investigated. The solution is obtained based on the infinite capillary theory via linear kinetic modeling described in the next section.

Closing the flow configuration description, it is useful to note that oscillatory pressure-driven gas flows, similar to the one formulated here, are realized in the hydrodynamic regime in several ways, including the oscillation of a piston [67] or a membrane [47] or even of the channel itself [43]. Good agreement between experimental and corresponding computational results, based on the fully developed assumption has been reported [46]. Similar setups are expected to be feasible also in the transition regime, where damping forces are reduced and the pressure gradient oscillation propagates easier through the channel, in a wide range of frequencies. Therefore, the flow characteristics are analyzed in the whole range of the gas rarefaction and oscillation frequency parameters. Obviously, any considerations or constraints present in viscous oscillatory pressure-driven flows setups must be also taken into account and reexamined in the case of rarefied gases.

III. KINETIC FORMULATION AND NUMERICAL SCHEME

The steady-state fully developed binary gas mixture flow between parallel plates, driven by pressure, temperature, and molar fraction gradients, in the whole range of gas rarefaction has been considered in [49]. Modeling has been based on McCormack kinetic model [30], which has been proven

to be a very reliable model, fulfilling all associated requirements (satisfies the conservation laws and the H-theorem and provides correct values for all transport coefficients). Here, the work follows the formulation in [49] related only to the pressure gradient part and it is accordingly extended to include the oscillatory flow behavior.

Due to the condition of small local pressure gradient ($X_P \ll 1$) the unknown time-dependent distribution function of each species can be linearized in a standard manner as

$$f_\alpha(t, x, y, \mathbf{c}_\alpha) = f_\alpha^0(\mathbf{c}_\alpha)[1 + X_P x \mathbb{R}(e^{-it}) + X_P \tilde{h}_\alpha(t, y, \mathbf{c}_\alpha)], \quad (35)$$

where

$$f_\alpha^0(\mathbf{c}_\alpha) = n_\alpha^{(A)} \left(\frac{m}{2\pi kT} \right)^{3/2} \exp[-\mathbf{c}_\alpha^2] \quad (36)$$

is the absolute Maxwellian of each species, $\tilde{h}_\alpha(t, y, \mathbf{c}_\alpha)$ are the unknown perturbed distribution functions and $\mathbf{c}_\alpha = [c_{\alpha x}, c_{\alpha y}, c_{\alpha z}]$ is the dimensionless molecular velocity vector, with $\alpha = 1, 2$ always denoting the light and heavy species, respectively. Furthermore, taking advantage of the harmonic motion, the complex distribution function $h_\alpha(y, \mathbf{c}_\alpha)$ is also introduced so that

$$\tilde{h}_\alpha(t, y, \mathbf{c}_\alpha) = \mathbb{R}[h_\alpha(y, \mathbf{c}_\alpha) \exp(-it)]. \quad (37)$$

Based on Eqs. (35) and (37), the problem under consideration may be formulated in terms of $h_\alpha(y, \mathbf{c}_\alpha)$ by the following system of two linearized Boltzmann equations:

$$-i \frac{\delta}{\theta} \sqrt{\frac{m_\alpha}{m}} h_\alpha + c_{\alpha y} \frac{\partial h_\alpha}{\partial y} = \omega_\alpha \sum_{\beta=1}^2 L_{\alpha\beta} h_\alpha - c_{\alpha x}, \quad \alpha = 1, 2. \quad (38)$$

In Eq. (38), $\omega_\alpha = \delta(C/\gamma_1 + (1-C)/\gamma_2)\sqrt{m_\alpha/m}$, with γ_α denoting the collision frequencies of each species and $L_{\alpha\beta}$ is the linearized McCormack collision term. Both $L_{\alpha\beta}$ and γ_α are identical to the ones specified in [49]. However, for self-containment purposes, they are also provided in the Appendix. It is noted that Eq. (38) depends not only on the ratio δ/θ , but also on the gas rarefaction parameter δ appearing in the expression for ω_α , with $\omega_\alpha \sim \delta$. Therefore, Eq. (38) depends on both δ and θ .

As it is well known, the z and x components of the molecular velocity vector may be eliminated, greatly reducing the computation effort of solving Eq. (38), by applying the so-called projection procedure and introducing the following reduced distribution functions:

$$\Phi_\alpha(y, c_{\alpha y}) = \frac{1}{\pi} \sqrt{\frac{m}{m_\alpha}} \int_{-\infty}^{\infty} \int_{-\infty}^{\infty} h_\alpha(y, \mathbf{c}_\alpha) c_{\alpha x} \exp[-c_{\alpha x}^2 - c_{\alpha z}^2] dc_{\alpha x} dc_{\alpha z}, \quad (39)$$

$$\Psi_\alpha(y, c_{\alpha y}) = \frac{1}{\pi} \sqrt{\frac{m}{m_\alpha}} \int_{-\infty}^{\infty} \int_{-\infty}^{\infty} h_\alpha(y, \mathbf{c}_\alpha) c_{\alpha x} (c_{\alpha x}^2 + c_{\alpha z}^2 - 2) \exp[-c_{\alpha x}^2 - c_{\alpha z}^2] dc_{\alpha x} dc_{\alpha z}. \quad (40)$$

Then, Eq. (38) is multiplied successively by the functions $\sqrt{m/m_\alpha} c_{\alpha x} \exp(-c_{\alpha x}^2 - c_{\alpha z}^2)/\pi$ and $\sqrt{m/m_\alpha} c_{\alpha x} (c_{\alpha x}^2 + c_{\alpha z}^2 - 2) \exp(-c_{\alpha x}^2 - c_{\alpha z}^2)/\pi$, and the resulting equations are integrated over $c_{\alpha x}$ and $c_{\alpha z}$ to deduce the following four coupled equations for the four unknown reduced complex distribution functions:

$$-i \frac{\delta}{\theta} \sqrt{\frac{m_\alpha}{m}} \Phi_\alpha + c_{\alpha y} \frac{\partial \Phi_\alpha}{\partial y} + \omega_\alpha \gamma_\alpha \Phi_\alpha - \frac{1}{2} \sqrt{\frac{m}{m_\alpha}} + \omega_\alpha \left\{ \gamma_\alpha u_\alpha - v_{\alpha\beta}^{(1)} (u_\alpha - u_\beta) - \frac{1}{2} v_{\alpha\beta}^{(2)} \left(q_\alpha - \frac{m_\alpha}{m_\beta} q_\beta \right) \right\}$$

$$\begin{aligned}
 & + 2\sqrt{\frac{m}{m_\alpha}} [(\gamma_\alpha - v_{\alpha\alpha}^{(3)} + v_{\alpha\alpha}^{(4)} - v_{\alpha\beta}^{(3)})\varpi_\alpha + v_{\alpha\beta}^{(4)}\varpi_\beta]c_{\alpha y} \\
 & + \frac{2}{5} \left[(\gamma_\alpha - v_{\alpha\alpha}^{(5)} + v_{\alpha\alpha}^{(6)} - v_{\alpha\beta}^{(5)})q_\alpha + v_{\alpha\beta}^{(6)}\sqrt{\frac{m_\beta}{m_\alpha}}q_\beta - \frac{5}{4}v_{\alpha\beta}^{(2)}(u_\alpha - u_\beta) \right] \left(c_{\alpha y}^2 - \frac{1}{2} \right), \quad (41)
 \end{aligned}$$

$$-i\sqrt{\frac{m_\alpha}{m}}\frac{\delta}{\theta}\Psi_\alpha + c_{\alpha y}\frac{\partial\Psi_\alpha}{\partial y} + \omega_\alpha\gamma_\alpha\Psi_\alpha = \frac{4}{5}\omega_\alpha \left[(\gamma_\alpha - v_{\alpha\alpha}^{(5)} + v_{\alpha\alpha}^{(6)} - v_{\alpha\beta}^{(5)})q_\alpha + v_{\alpha\beta}^{(6)}\sqrt{\frac{m_\beta}{m_\alpha}}q_\beta - \frac{5}{4}v_{\alpha\beta}^{(2)}(u_\alpha - u_\beta) \right]. \quad (42)$$

In Eqs. (41) and (42) $\alpha, \beta = 1, 2$, with $\alpha \neq \beta$, while the expressions for the quantities $v_{\alpha\beta}^{(k)}$ are implemented based on the intermolecular model potential. In steady pressure-driven flows of single gases and binary gas mixtures through capillaries, the effect of the intermolecular potential model is very small. In gas mixture flows, this has been clearly demonstrated by comparing the species flow rates based on the hard sphere model, with corresponding ones based on realistic [49], *ab initio* [68] and Lennard-Jones [69] potentials. As stated in Sec. IV, this is also valid in the present oscillatory, isothermal, fully developed flow, and therefore the expressions for the quantities $v_{\alpha\beta}^{(k)}$ in Eqs. (41) and (42), are based on the hard sphere model, which is the simplest one, and are given in the Appendix.

The macroscopic quantities u_α , ϖ_α and q_α at the right-hand side of Eqs. (41) and (42) are defined in Eqs. (17), (18), and (19), respectively, and after applying the linearization and projection procedures, they are obtained as moments of Φ_α and Ψ_α as follows:

$$u_\alpha(y) = \frac{1}{\sqrt{\pi}} \int_{-\infty}^{\infty} \Phi_\alpha \exp(-c_{\alpha y}^2) dc_{\alpha y}, \quad (43)$$

$$\varpi_\alpha(y) = \frac{1}{\sqrt{\pi}} \sqrt{\frac{m_\alpha}{m}} \int_{-\infty}^{\infty} \Phi_\alpha c_{\alpha y} \exp(-c_{\alpha y}^2) dc_{\alpha y}, \quad (44)$$

$$q_\alpha(y) = \frac{1}{\sqrt{\pi}} \int_{-\infty}^{\infty} \left[\Psi_\alpha + \left(c_{\alpha y}^2 - \frac{1}{2} \right) \Phi_\alpha \right] \exp(-c_{\alpha y}^2) dc_{\alpha y}. \quad (45)$$

In the present work purely diffuse reflection at the walls is assumed. It is readily deduced that the outgoing reduced distribution functions at the two walls are identically equal to zero:

$$\Phi_\alpha(\pm 1/2, c_{\alpha y}) = \Psi_\alpha(\pm 1/2, c_{\alpha y}) = 0, \quad c_{\alpha y} \gtrless 0. \quad (46)$$

Thus, the kinetic formulation of the problem is properly defined by the system of Eqs. (41) and (42), subject to the boundary conditions (46), along with the associated moments (43)–(45).

It is interesting to analyze the behavior of Eqs. (41) and (42) at limiting values of all involved parameters. As $\theta \rightarrow \infty$ ($\omega \rightarrow 0$), the inertia terms (first terms at the left-hand side of the equations), along with the imaginary part of the distribution function and all associated macroscopic quantities tend to zero and (41) and (42) tend to the corresponding steady-state ones in [49]. In steady-state conditions the ratio G_1/G_2 decreases monotonically from $\sqrt{m_2/m_1}$ in the free molecular regime down to one in the viscous regime. At the other end, in the very high oscillation frequency regime, as $\theta \rightarrow 0$, a scale analysis is performed to deduce that the inertia terms

of Eqs. (41) and (42) and the source term at the right-hand side of Eq. (41) tend to zero in a slower pace than all other terms yielding that

$$\lim_{\theta \rightarrow 0} \Phi_\alpha = -i\frac{\theta}{2\delta}\frac{m}{m_\alpha} \quad \text{and} \quad \lim_{\theta \rightarrow 0} \Psi_\alpha = 0. \quad (47)$$

Substituting Eq. (47) into Eq. (43)–(45) it is seen that as $\theta \rightarrow 0$, $u_\alpha = -i(\theta/2\delta)(m/m_\alpha)$, $\varpi_\alpha = 0$ and $q_\alpha = 0$. Also, from Eq. (21) the flow rates are $G_\alpha = -i(\theta/\delta)(m/m_\alpha)$, while the flow rate ratio of the species is $G_1/G_2 = m_2/m_1$. In addition, it is readily seen that as $\theta \rightarrow 0$, the amplitude of all quantities is diminishing, while their phase angle tends to $\pi/2$. Furthermore, with regard to the gas rarefaction parameter, as $\delta \rightarrow 0$, with $\theta > 0$, Eqs. (41) and (42) tend to the corresponding ones for steady-state binary gas flow in the free molecular limit [49], while the flow is in the hydrodynamic regime when both $\delta \gg 1$ and $\theta \gg 1$. Also, for $C = 0$ or for binary gas mixtures with species having the same molecular mass $m_1 = m_2$, Eqs. (41) and (42) are reduced to the corresponding ones for oscillatory single gas flow [9]. All these remarks, including the analysis in the high oscillation frequency regime, are considered in the computational results to explain the flow behavior and for benchmarking purposes.

The above set of equations is computationally solved based on the discrete velocity method [12] in the c_y space and on the second-order diamond finite difference scheme [50] in the y space. The continuum spectrum of $c_y \in (-\infty, \infty)$ is properly transferred to $[0, \infty)$, and then, it is replaced by a set of discrete velocities $m = 1, 2, \dots, M$, which are taken to be the roots of the Hermite polynomial of order M , accordingly mapped from $(-\infty, \infty)$ to $[0, \infty)$. The macroscopic distributions are numerically integrated by the Gauss-Hermite quadrature scheme. The specific set of discrete molecular velocities has been found to be very effective in the whole range of gas rarefaction. The discretized equations are solved in an iterative manner between the kinetic equations (41) and (42) and the moment equations (43)–(45). Since the computed quantities are complex their real and imaginary parts are obtained. The iteration map is concluded when the following criterion in terms of the bulk velocity and the heat flow of the species is fulfilled:

$$\begin{aligned}
 \varepsilon_j^{(\kappa)} = \max_i \{ & |u_{1,j,i}^{(\kappa)} - u_{1,j,i}^{(\kappa-1)}| + |u_{2,j,i}^{(\kappa)} - u_{2,j,i}^{(\kappa-1)}| \\
 & + |q_{1,j,i}^{(\kappa)} - q_{1,j,i}^{(\kappa-1)}| + |q_{2,j,i}^{(\kappa)} - q_{2,j,i}^{(\kappa-1)}| \} < \varepsilon. \quad (48)
 \end{aligned}$$

Here, ε is the tolerance parameter, the superscript (κ) is the iteration index, the subscript $j = \mathbb{R}, \mathbb{I}$ refers to the real and imaginary part of the macroscopic quantity and the subscript $i = 1, 2, \dots, I$ refers to the node number in $y \in [-1/2, 1/2]$. The numerical parameters have been gradually refined to

ensure grid independent results up to several significant figures. The implemented computational scheme has been previously successfully applied to steady-state binary gas mixture and oscillatory single gas flows [9,10,49,50].

Once the real and imaginary part of the macroscopic distributions and of the associated overall quantities (e.g., flow rates) are obtained, it is straightforward to compute their amplitudes and phase angles, as well as the corresponding time-dependent quantities, presented and discussed in the next section.

IV. RESULTS AND DISCUSSION

Computational results for the velocity and shear stress distributions, flow rates and some complimentary quantities (wall shear stress and pumping power) are presented in Sec. IV A, IV B, and IV C, respectively, in a wide range of the gas rarefaction and oscillation parameters δ and θ , as well as of the molar fraction $C \in [0, 1]$ and molecular mass ratio of the heavy over the light species m_2/m_1 . Although several binary gas mixtures have been considered, the effect of m_2/m_1 is demonstrated by presenting results only for He-Xe, with $m_2/m_1 = 32.8$ and Ne-Ar, with $m_2/m_1 = 1.98$, while the corresponding molecular diameter ratios d_2/d_1 are 2.226 and 1.406. The molecular diameter ratios have been obtained via Eq. (35) in [70] using the viscosity data in [71]. To better demonstrate the flow characteristics in oscillatory binary gas mixture flow, comparisons between the present results and the corresponding ones for steady-state binary gas flow in [49] and oscillatory single gas flow in [9] are performed.

All presented results are based on the hard sphere model. However, in order to examine the effect of the intermolecular potential, in addition to the hard sphere model, the realistic potential model [49] has been also employed. In all cases small discrepancies between the two models are observed and they are always smaller than the corresponding steady ones. It is concluded that in oscillatory pressure-driven fully developed binary gas mixture flows, as in the steady ones, the effect of the intermolecular potential is very small and therefore, the associated results based on the realistic potential are not included.

The accuracy of the computational scheme and the presented results has been accordingly validated by always fulfilling the benchmark balance expression (32), as well as by systematic comparisons with corresponding computational and analytical results at the following limiting values of the involved parameters: (a) steady-state binary gas mixture flow ($\theta \rightarrow \infty$), (b) oscillatory single gas flow ($C = 0$), (c) high oscillation frequency regime ($\theta \rightarrow 0$), and (d) oscillatory gas mixture flow in hydrodynamic regime ($\delta, \theta \gg 1$). The numerical grid is properly refined to ensure grid independent results up to certain number of significant figures. The presented numerical results are with $M = 128$ discrete velocities, $I = 10^4$ physical nodes and tolerance parameter $\varepsilon = 10^{-8}$. It is confirmed that by successively increasing the number of discrete velocities to $M = 256$ and 512, as well as the number of nodes to $I = 2 \times 10^4$ and 4×10^4 , does not alter the flow rate of the species more than 0.1% in the whole range of the involved parameters (C, θ, δ) and for all tested gas mixtures. Therefore, the aforementioned numerical parameters $M = 128, I = 10^4$,

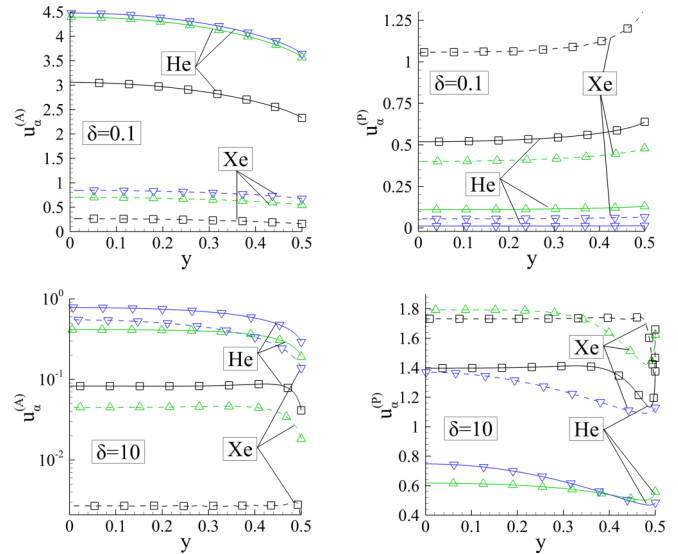


FIG. 1. Velocity amplitude $u_\alpha^{(A)}(y)$ and phase angle $u_\alpha^{(P)}(y)$ (rad) of each species of He-Xe, with $C = 0.5$, for $\delta = [0.1, 10]$ and $\theta = 0.1$ (\square), $\theta = 1$ (\triangle), $\theta = 10$ (∇) (He: solid lines, Xe: dashed lines).

are considered as adequate to capture the effects described in the paper. All results are in dimensionless form.

A. Velocity and shear stress distributions

The amplitude and phase angle of the complex velocity $u_\alpha = u_\alpha^{(A)} \exp(iu_\alpha^{(P)})$ of the species of the He-Xe gas mixture are reported in Figs. 1, 2, and 3 for various values of δ, θ and C . Also, in Fig. 3 some shear stress distributions $\varpi_\alpha = \varpi_\alpha^{(A)} \exp(i\varpi_\alpha^{(P)})$ are included.

In Fig. 1 the distributions of the velocity amplitude $u_\alpha^{(A)}(y)$ and phase angle $u_\alpha^{(P)}(y)$ of each species of the He-Xe gas mixture, with $C = 0.5$, are provided for $\delta = [0.1, 10]$ and $\theta = [0.1, 1, 10]$. The distributions of He and Xe present the same qualitative behavior in terms of the gas rarefaction and oscillation parameters, and they both also have a close qualitative resemblance with corresponding results for oscillatory single gas flows [9,10]. Very briefly, it is observed that as θ is decreased, the amplitude $u_\alpha^{(A)}$ is decreased, while the phase angle $u_\alpha^{(P)}$ is increased. It is also seen that at small δ and large θ (e.g., $\delta = 0.1$ and $\theta \geq 1$) the velocity amplitudes have the expected shape with their maximum appearing at the center of the flow field, while at large δ and small θ (e.g., $\delta = 10$ and $\theta \leq 1$) the velocity amplitudes are flattening in the core of the flow and the maximum amplitudes are appearing in thin layers adjacent to the walls. The corresponding phase angles in the former case are small, while in the latter one are large close to the limiting value of $\pi/2$. This is the so-called “velocity overshooting” or “Richardson effect,” well known for a long time in oscillatory viscous flows [3] and recently reported in oscillatory rarefied gas flows [9,10]. The overall behavior is due to the combined rarefaction and inertia effects. In the present work, the investigation is focused in comparing the above described flow patterns and characteristics between the light and heavy species of the mixture.

It is readily seen, in Fig. 1 that the velocity amplitudes of He are always about one order of magnitude larger than

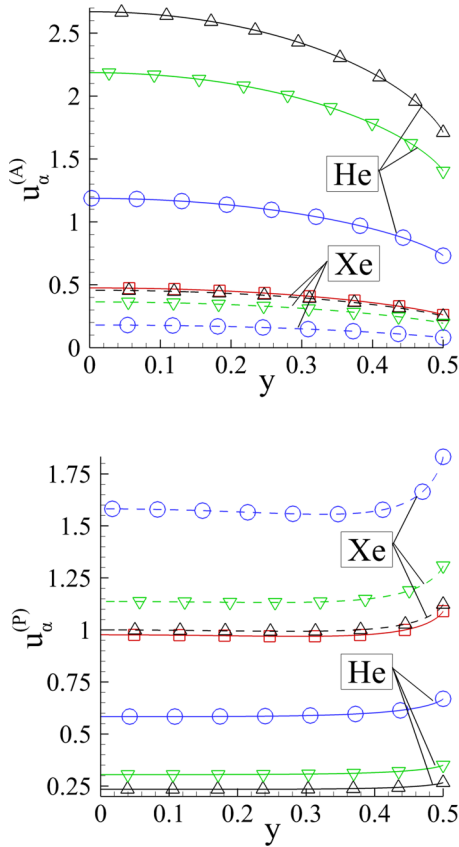


FIG. 2. Velocity amplitude $u_{\alpha}^{(A)}(y)$ and phase angle $u_{\alpha}^{(P)}(y)$ (rad) of each species of He-Xe, with $C = 0$ (\square), $C = 0.1$ (Δ), $C = 0.5$ (∇), $C = 0.9$ (\circ), for $\delta = 1$ and $\theta = 1$ (He: solid lines, Xe: dashed lines).

the corresponding ones of Xe. It is well known from investigations in steady-state binary gas mixture flows that lighter species travel faster than heavier ones, resulting in gas separation, which is increased as the gas flow becomes more rarefied [49,50]. Therefore, the present results are expected. However, it is interesting to note that as θ decreases, i.e., as the oscillation frequency increases, the relative difference between the velocity amplitudes of the light and heavy species increases. This becomes more evident at $\delta = 10$, where the amplitudes of He and Xe for $\theta = 10$ are relatively close to each other, since the flow is close to the hydrodynamic regime, while for $\theta = 1$ and 0.1 the difference between them is gradually increased. On the contrary, the velocity phase angles of He are always smaller than the corresponding ones of Xe. In general, the velocity phase angles are increased as θ is decreased. It may be stated that as the oscillation frequency is increased the velocity amplitude and phase angle of both species is decreased and increased respectively. Clearly, however, the difference between the velocity amplitudes of the light and heavy species is increased with the oscillation frequency, not only for small but also for large values of the gas rarefaction parameter. It seems that in oscillatory gas mixture flows, gas separation may be intensified as the oscillation frequency is increased due to inertia forces, which affect differently the light and heavy species. These remarks are in agreement with the analytical results, given in Sec. III, as $\theta \rightarrow 0$ and are

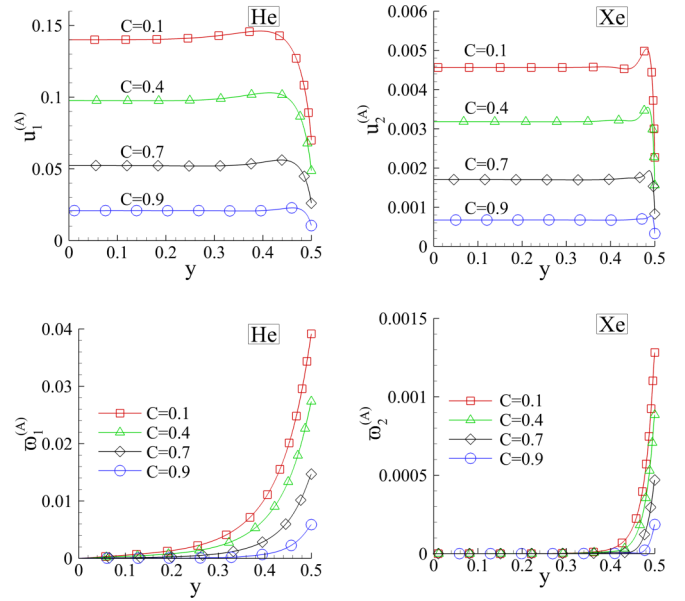


FIG. 3. Velocity and shear stress amplitudes $u_{\alpha}^{(A)}(y)$ and $w_{\alpha}^{(A)}(y)$ of each species of He-Xe, with $C = [0.1, 0.4, 0.7, 0.9]$ for $\delta = 10$ and $\theta = 0.1$.

further investigated in the next subsection in terms of the species flow rates.

In Fig. 2 the distributions of the velocity amplitude $u_{\alpha}^{(A)}(y)$ and phase angle $u_{\alpha}^{(P)}(y)$ of each species of the He-Xe gas mixture, with $C = [0, 0.1, 0.5, 0.9]$, are provided for $\delta = 1$ and $\theta = 1$. Here, the effect of the molar fraction on the velocity amplitude and the phase angle is investigated for typical values of the gas rarefaction and oscillation parameters. The case of $C = 0$ corresponds to oscillatory single gas flow. As C is increased from 0.1 to 0.9 , i.e., the molar fraction of the light species (He) is increased, the velocity amplitudes and phase angles of both species are decreased and increased, respectively. Of course, as $C \rightarrow 1$, the single gas flow results ($C = 0$) are recovered [49,50]. It is noted that the changes in $u_1^{(A)}(y)$ and $u_1^{(P)}(y)$ of He in terms of C , compared to the corresponding ones $u_2^{(A)}(y)$ and $u_2^{(P)}(y)$ of Xe, both qualitatively and quantitatively, on a relative base, are about the same. This behavior remains the same in the whole range of gas rarefaction and oscillation parameters.

In Fig. 3 the distributions of the velocity and shear stress amplitudes $u_{\alpha}^{(A)}(y)$ and $w_{\alpha}^{(A)}(y)$ of each species of the He-Xe gas mixture, with $C = [0.1, 0.4, 0.7, 0.9]$, are provided for $\delta = 10$ and $\theta = 0.1$. The specific values of the gas rarefaction and oscillation parameters, associated with high-frequency oscillatory flow between the transition and slip flow regimes, are suitable for investigating the velocity overshooting phenomenon in the components of the two mixtures. Observing the velocity amplitudes of He and Xe, it is evident that with these flow parameters, velocity overshooting is always present (all C). For Xe, compared to He, the velocity overshooting becomes sharper appearing, along with its maximum value, closer to the wall inside a much thinner layer. In the core of the flow, the flat velocity amplitudes of both He and Xe are very close to the corresponding analytical amplitudes $u_{\alpha}^{(A)} = (\theta/2\delta)(m/m_{\alpha})$ obtained in Sec. III. In parallel, the shear stress

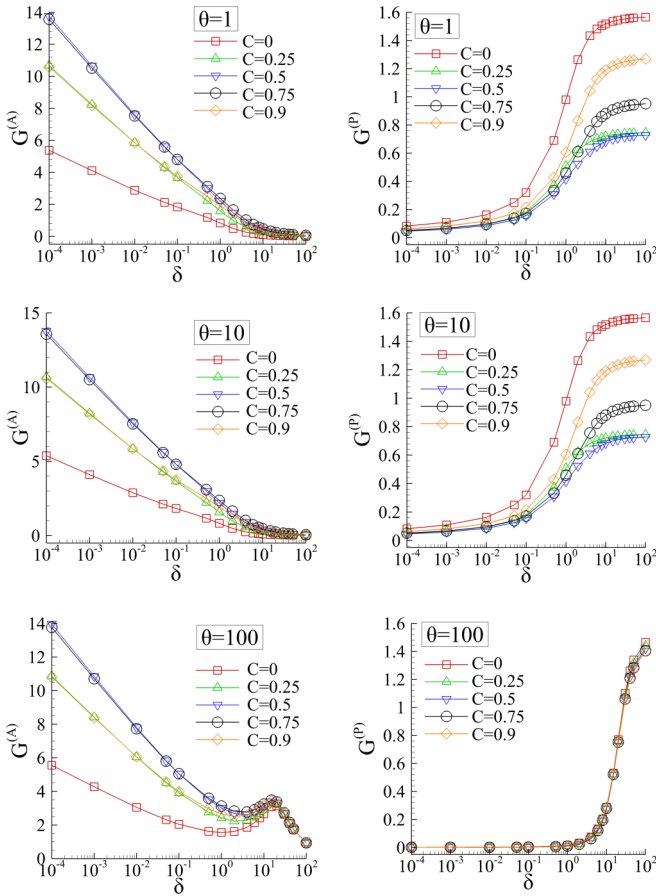


FIG. 4. Mixture flow rate amplitude $G^{(A)}$ and phase angle $G^{(P)}$ (rad) of He-Xe in terms of $\delta \in [10^{-4}, 10^2]$, with $C = [0, 0.25, 0.5, 0.75, 0.9]$ and $\theta = [1, 10, 10^2]$.

amplitudes for both He and Xe take their highest values at the wall, and they are monotonically decreased towards the channel center. The attenuation of the shear stress amplitude of He is smoothly diffused in the whole distance from the wall to the center, while the one of Xe is rapid in a narrow zone close to the wall and far from the wall the shear stress of Xe becomes zero. This description of the velocity and shear stress amplitudes remains valid for all molar fractions tested. As it is well known, velocity overshooting is due to the fact that close to the wall viscous and pressure gradient forces actually add to each other due to the large phase angle lag between them. As a result, the combined effect accelerates the fluid to higher velocities than those produced in the core by the pressure gradient forces acting alone [66]. Therefore, since the viscous forces in the case of He act in the whole distance between the plates, while in the case of Xe only in thin zones close to the walls, the above observations on the velocity overshooting of He and Xe are both physically and computationally justified. Corresponding results for other mixtures (e.g., Ne-Ar, He-Ar) have a similar behavior. Therefore, it is stated that as the molecular mass of the gas species increases, the species shear stress, which is created at the wall and diffused into the flow, attenuates more rapidly. In parallel, the Stokes layer becomes thinner and the Richardson effect more pronounced.

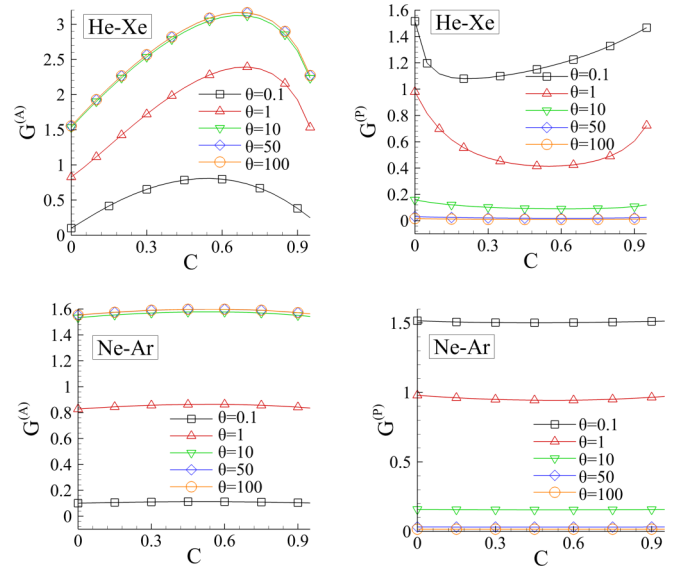


FIG. 5. Mixture flow rate amplitude $G^{(A)}$ and phase angle $G^{(P)}$ (rad) of He-Xe and Ne-Ar in terms of the molar fraction C for $\delta = 1$ and $\theta = [10^{-1}, 1, 10, 50, 10^2]$.

Having obtained a description of the dependency of the velocity distribution of each species of the binary gas mixture on the molecular masses and molar fraction in a wide range of the flow parameters, in the next section the corresponding behavior of the flow rates is investigated.

B. Flow rates of the mixture and the species

The reported results include the complex flow rates of the mixture $G = G^{(A)} \exp(iG^{(P)})$ (Figs. 4 and 5) and of the species $G_\alpha = G_\alpha^{(A)} \exp(iG_\alpha^{(P)})$ (Figs. 6, 7, and 8), as well as of the time-dependent flow rate $\tilde{G}(t) = G^{(A)} \cos[t - G^{(P)}]$ (Fig. 9). The effect of the oscillation frequency on the gas separation phenomenon is investigated by computing the amplitude ratio $G_1^{(A)}/G_2^{(A)}$ and the phase angle difference $G_2^{(P)} - G_1^{(P)}$ of the two species.

In Fig. 4 the He-Xe flow rate amplitude $G^{(A)}$ and phase angle $G^{(P)}$ are provided in terms of $\delta \in [10^{-4}, 10^2]$, with $\theta = [1, 10, 10^2]$ and $C = [0, 0.25, 0.5, 0.75, 0.9]$. The results for oscillatory single gas flow ($C = 0$), previously reported in [9], are also included here for comparison purposes. It is seen that the flow rate amplitudes and phase angles of the mixture ($C \neq 0$) depend on the flow parameters very similarly to the corresponding single gas ones ($C = 0$). The behavior of the single gas flow rate in terms of the flow parameters has been analyzed in detail in [10], and it remains the same in the binary gas mixture flow and therefore is not repeated here. It is only pointed out that as θ decreases (the oscillation frequency increases), the flow rate amplitude decreases and phase angle increases. Focusing on the effect of the molar fraction, it is seen that always the mixture flow rate amplitude is larger and the phase angle is smaller than the corresponding ones of the single gas. Also, $G^{(A)}$ and $G^{(P)}$ vary nonmonotonically with C . More specifically, as C is increased, $G^{(A)}$ is initially increased until the molar fraction is in the range of $C \in [0.5, 0.75]$, and then it is decreased to reach the single gas

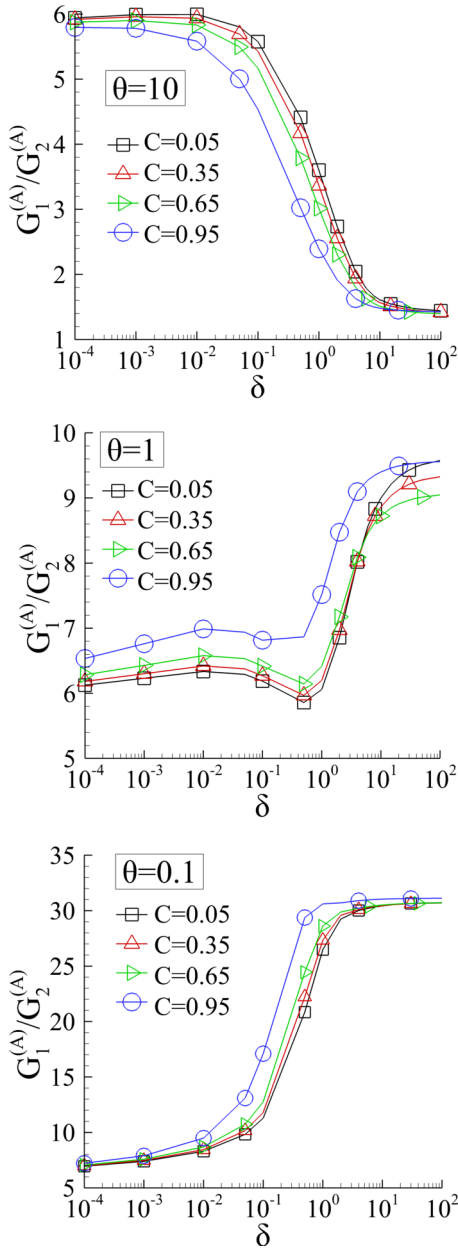


FIG. 6. Ratio of flow rate amplitudes $G_1^{(A)}/G_2^{(A)}$ of the species of He-Xe in terms of $\delta \in [10^{-4}, 10^2]$, with $C = [0.05, 0.35, 0.65, 0.95]$ and $\theta = [0.1, 1, 10]$.

one, while $G^{(P)}$ varies in the opposite way, i.e., first decreases and then increases. It is noted that the effect of C on $G^{(A)}$ remains significant in all oscillation regimes, while its effect on $G^{(P)}$ is important only in high and moderate frequencies and becomes negligible at low frequencies. At large values of the gas rarefaction parameter ($\delta \geq 10$) the effect of C is gradually diminished.

A more detailed view of the effect of the molar fraction on the mixture flow rate is shown in Fig. 5, where its amplitude $G^{(A)}$ and phase angle $G^{(P)}$ are provided for He-Xe and Ne-Ar in terms of C for many values of $\theta = [0.1, 1, 10, 50, 10^2]$ and the typical value of $\delta = 1$. In the case of He-Xe, the non-monotonic behavior of $G^{(A)}$ and $G^{(P)}$ in terms of C , along with its dependency on θ , are clearly demonstrated. It is seen

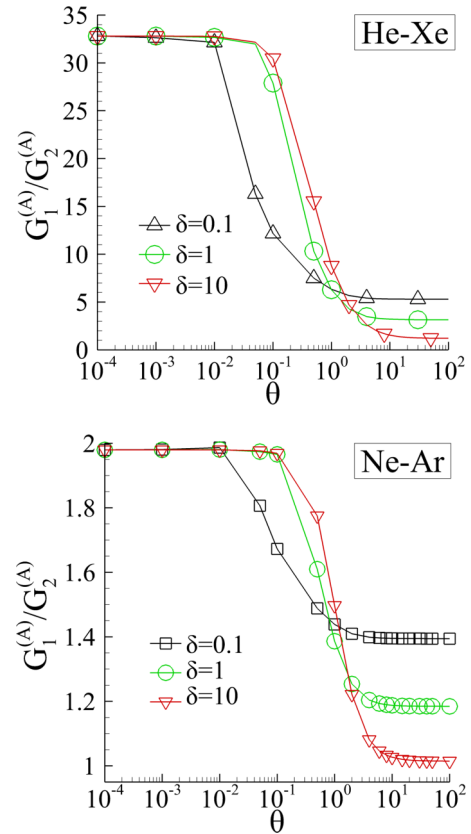


FIG. 7. Ratio of flow rate amplitudes $G_1^{(A)}/G_2^{(A)}$ of the species of He-Xe and Ne-Ar, with $C = 0.5$, in terms of $\theta \in [10^{-4}, 10^2]$ for $\delta = [0.1, 1, 10]$.

that the amplitude $G^{(A)}$ strongly depends on C for all θ , but it varies more significantly as the oscillation parameter is increased. The phase angle $G^{(P)}$ depends on C for small values of θ , while it is practically independent of C for $\theta \geq 10$. This behavior remains qualitative the same in the whole range of gas rarefaction, with the general observation that the effect of the molar fraction is more pronounced as δ decreases and the flow becomes more rarefied. Also, as δ increases the maximum flow amplitude appears at larger C . In the case of Ne-Ar both the amplitude and the phase angle depend very weakly in the molar fraction since the molecular masses of Ne and Ar are much closer to each other than of He and Xe. Also, the flow rate amplitude and phase angle of Ne-Ar are smaller and larger respectively, compared to the corresponding ones of He-Xe.

The investigation is continued by considering the amplitudes and the phase angles of the mixture components in terms of C and m_2/m_1 , which are of particular interest in investigating the gas separation phenomenon for various values of δ and θ . In Fig. 6 the ratio of the flow rate amplitudes $G_1^{(A)}/G_2^{(A)}$ is provided in terms of $\delta \in [10^{-4}, 10^2]$ for the He-Xe gas mixture, with $C = [0.05, 0.35, 0.65, 0.95]$ and $\theta = [0.1, 1, 10]$. At $\theta = 10$ the ratio $G_1^{(A)}/G_2^{(A)}$ varies qualitatively similarly as in the steady-state binary gas flow setup. At very low values of δ it is close to the limiting value $\sqrt{m_2/m_1} = 5.73$. Then, it is about constant or slightly reduced in the free molecular regime and it is decreased in the transition regime, reaching finally,

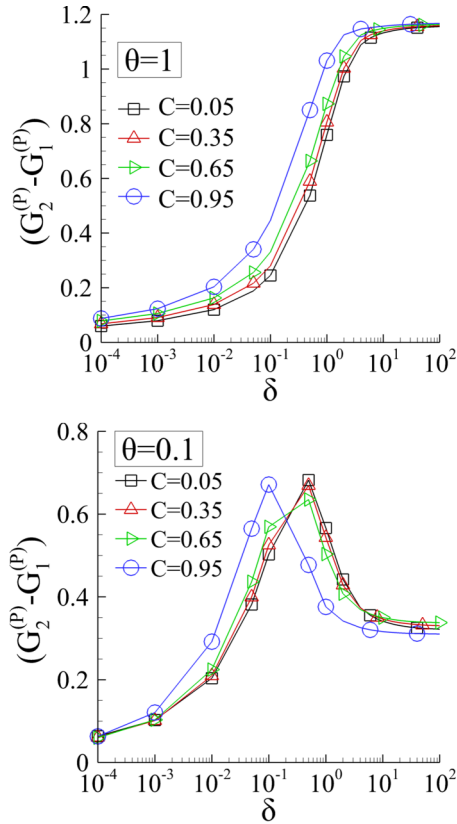


FIG. 8. Difference of the flow rate phase angles $G_2^{(P)} - G_1^{(P)}$ (rad) of the species of He-Xe in terms of $\delta \in [10^{-4}, 10^2]$, with $C = [0.05, 0.35, 0.65, 0.95]$ and $\theta = [0.1, 1]$.

in the slip and hydrodynamic regimes, asymptotically to one. However, at $\theta = 1$ and $\theta = 0.1$ the behavior of $G_1^{(A)}/G_2^{(A)}$ is completely different. It remains about constant in free molecular regime, but then, it is increased in the transition regime and finally, as δ further increases, it keeps asymptotically increasing to some constant value. This behavior, with the minimum and maximum values of $G_1^{(A)}/G_2^{(A)}$ appearing at the free molecular and hydrodynamic limits, respectively, and the increase in the transition regime (completely reversed compared to the steady-state behavior) becomes more pronounced as θ is decreased. It is evident that the oscillation parameter θ has a dominant effect on the amplitude ratio of He over Xe, which is significantly increased as θ is decreased (at $\theta = 0.1$ the flow rate amplitude of He is about 30 times larger than of Xe). This behavior is due to the corresponding behavior of the velocity amplitudes commented in Fig. 1, and it is contributed to inertia forces, which are increased with the oscillation frequency, and they influence the bulk velocity amplitude of the heavy species much more than of the light one. Therefore, as θ is decreased, the flow rate amplitude of the heavy species decreases much more significantly than the light one, and although both amplitudes are decreased the velocity amplitude ratio of the light over the heavy species is increased. This effect is magnified in the transition regime, as the flow becomes less rarefied overcoming diffusion effects due to increased intermolecular collisions and therefore as δ increases the amplitude ratio keeps increasing. It is seen that

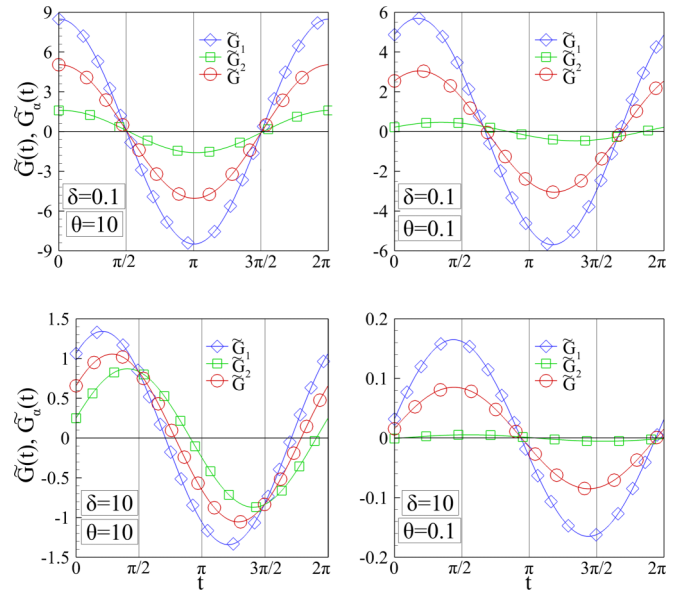


FIG. 9. Time-dependent flow rates $\tilde{G}_1(t)$ of He, $\tilde{G}_2(t)$ of Xe and $\tilde{G}(t)$ of He-Xe, with $C = 0.5$, over one cycle $t \in [0, 2\pi]$ for $\delta = [0.1, 10]$ and $\theta = [0.1, 10]$.

the effect of C with regard to these flow characteristics is rather small and becomes even smaller as the oscillation frequency is increased (θ is decreased). In general, the amplitude ratio is slightly increased with the molar fraction.

The ratio of flow rate amplitudes $G_1^{(A)}/G_2^{(A)}$ is presented again in Fig. 7 in terms of $\theta \in [10^{-4}, 10^2]$ for the He-Xe and Ne-Ar gas mixtures, with $C = 0.5$ and $\delta = [0.1, 1, 10]$. At high oscillation frequencies ($\theta \leq 10^{-2}$), although the flow rate amplitude of each species is decreased, the ratios of the species amplitudes take their highest values, which are almost constant independent of the gas rarefaction parameter δ and equal, as it is numerically found, with the molecular mass ratio of the heavy over the light species m_2/m_1 ($G_{He}^{(A)}/G_{Xe}^{(A)} = 32.8$, $G_{Ne}^{(A)}/G_{Ar}^{(A)} = 1.98$). This is in accordance to the corresponding analytical expressions in Sec. III, where as $\theta \rightarrow 0$, $G_1/G_2 = m_2/m_1$. Then, at moderate oscillation frequencies ($10^{-2} < \theta < 10$) the amplitude ratio is decreased in all gas rarefaction regimes. Finally, at small oscillation frequencies ($\theta \geq 10$) the corresponding steady-state results are asymptotically recovered. Obviously in oscillatory flows the effect of the molecular mass ratio m_2/m_1 on the ratio of the flow rate amplitude of the light over the heavy species is dominant in the whole range of gas rarefaction.

In Fig. 8 the difference of the flow rate phase angles $G_2^{(P)} - G_1^{(P)}$ is provided in terms of $\delta \in [10^{-4}, 10^2]$ for the He-Xe gas mixture, with $C = [0.05, 0.35, 0.65, 0.95]$ and $\theta = [0.1, 1]$. At $\theta = 1$, as well as for $\theta > 1$ (not shown here), the difference of the flow rate phase angles $G_2^{(P)} - G_1^{(P)}$ is monotonically increased with δ , with the increase mostly occurring at intermediate values of δ in the transition regime. This is not the case at $\theta = 0.1$, where the difference $G_2^{(P)} - G_1^{(P)}$ is first increased, reaching some maximum value in the transition regime, and then it is decreased reaching asymptotically some constant value. This behavior is also present at $\theta < 0.1$ (not shown here), with the maximum value appearing at lower δ , as

θ is decreased. In general, it is demonstrated that there is phase angle difference between the flow rates of the two species of the mixture.

In Fig. 9 the phase lag between the oscillatory pressure gradient and flow rates of each species and the mixture is demonstrated, by plotting the time-dependent flow rates $\tilde{G}_1(t)$ of He, $\tilde{G}_2(t)$ of Xe, as well as $\tilde{G}(t) = C\tilde{G}_1(t) + (1 - C)\tilde{G}_2(t)$ of the He-Xe gas mixture with $C = 0.5$, over one cycle $t \in [0, 2\pi]$ for $\delta = [0.1, 10]$ and $\theta = [0.1, 10]$. It is noted that the dimensionless time-dependent pressure gradient is equal to $\cos(t)$. In the case $\theta = 10$ (low oscillation frequency) and $\delta = 0.1$ all quantities are in phase to each other, and as δ is increased they are gradually getting out of phase (at $\delta = 10$ they are out of phase). In the case $\theta = 0.1$ (high oscillation frequency) and $\delta = 0.1$ all quantities are almost in phase to each other. Again the phase lag is further increased with δ and at $\delta = 10$ the phase angle lag is almost equal to $\pi/2$. Always, the phase angle lag of the flow rate of Xe is larger than the one of He, and the phase lag of the mixture flow rate is, as expected, between the phase lags of the two species, while the amplitudes of the oscillatory He flow rate are much larger than the corresponding ones of Xe. It is noted that results obtained with the same ratio δ/θ vary to each other for different values of δ [10]. This is well expected since the governing equations depend on both δ and θ , and not only on the ratio δ/θ , with the effect of the inertia forces attenuating as the flow becomes more rarefied. All these remarks are in agreement with the discussion presented in terms of the amplitudes and the phase angles of the species flow rates in Figs. 6–8. Overall, it may be stated that the oscillatory flow rates and pressure gradient are in phase when $\delta \ll \theta$ and completely out of phase when $\theta \ll \delta$, with the heavier species have larger phase angle lags compared to the lighter ones.

It is noted that the flow rates of other mixtures (e.g., He-Ar), as well as of their species, have been computed, in the whole range of the molar fraction and for various values of the flow parameters. The flow rate amplitude ratio $G_1^{(A)}/G_2^{(A)}$ and phase angle difference $G_2^{(P)} - G_1^{(P)}$ of the species of all binary gas mixtures tested have a close resemblance with the corresponding ones for He and Xe. However, quantitatively the results are different with the values of $G_1^{(A)}/G_2^{(A)}$ and $G_2^{(P)} - G_1^{(P)}$ becoming much smaller and gradually independent of C , as the molecular mass ratio m_2/m_1 is decreased, recovering the oscillatory single gas behavior as $m_2/m_1 \rightarrow 1$. This remark, well known in steady-state flows, remains valid also in oscillatory gas mixture flows. Characteristic is the case of Ne-Ar, with molecular mass ratio equal to about two, where for $\delta = [0.1, 1, 10]$ and $\theta \in [10^{-1}, 10^2]$, the flow rate amplitude $G^{(A)}$ and the phase angle $G^{(P)}$ of the mixture in terms of C , are becoming flat completely independent of the molar fraction. The results for He-Ar, Ne-Ar, and other mixtures of monatomic gases are not presented here, but they are available upon request.

Probably, the most interesting finding concerning the flow rates is that, independent of the molar fraction and gas rarefaction regime, the amplitude ratio of the oscillatory flow rates of the light over the heavy species is significantly increased as the oscillation frequency is increased. Clearly, these results may be of major technological importance in

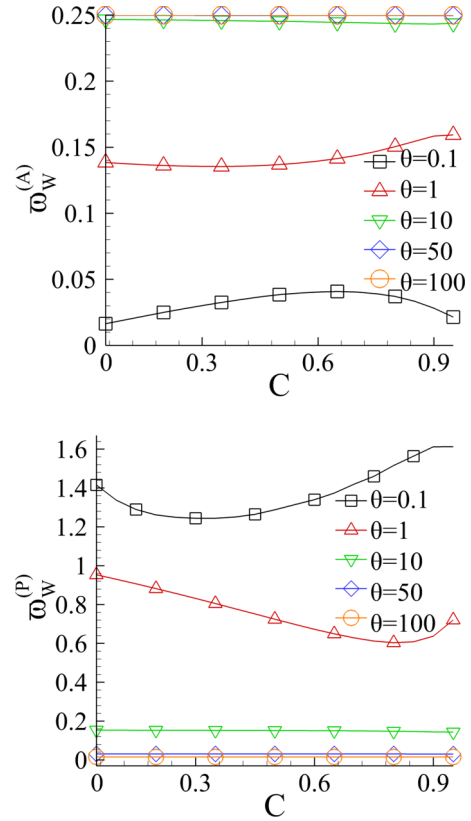


FIG. 10. Wall shear stress amplitude $\varpi_W^{(A)}$ and phase angle $\varpi_W^{(P)}$ (rad) of He-Xe in terms of C for $\theta = [0.1, 1, 10, 50, 10^2]$ and $\delta = 1$.

several technological applications, including the development of gas separation apparatus in the whole range of the Knudsen number.

C. Wall shear stress and pumping power

Complementary quantities of the oscillatory binary gas mixture of practical interest, namely the wall shear stress $\varpi_W = \varpi_W^{(A)} \exp(i\varpi_W^{(P)})$ (Fig. 10), as well as the oscillatory cycle-average pumping power \bar{E} (Fig. 11), given by Eq. (27), are here considered.

In Fig. 10 the wall shear stress amplitude $\varpi_W^{(A)}$ and phase angle $\varpi_W^{(P)}$ are provided in terms of $C \in [0, 1]$ for $\theta = [0.1, 1, 10, 50, 10^2]$ and the typical value of $\delta = 1$. It is readily seen that as the molar fraction varies between zero and one, both the wall shear stress amplitude and phase angle remain constant for $\theta = [10, 50, 10^2]$ and vary slightly for $\theta = [0.1, 1]$. It is evident that the dependency of the shear stress on the molar fraction is very weak and this behavior remains the same in the whole range of gas rarefaction. As expected $\varpi_W^{(A)}$ is decreased and $\varpi_W^{(P)}$ is increased as θ is decreased. Actually, $\varpi_W^{(A)}$ almost diminishes at very high oscillation frequencies. Furthermore, as θ is increased and the oscillation frequency tends to zero, the shear stress amplitude $\varpi_W^{(A)}$ approaches the limiting value of 0.25, which is the steady-state dimensionless wall shear stress, independent of δ [72], while the shear stress phase angle $\varpi_W^{(P)}$ approaches zero. These results further validate the accuracy of the present oscillatory binary gas mixture computational approach.

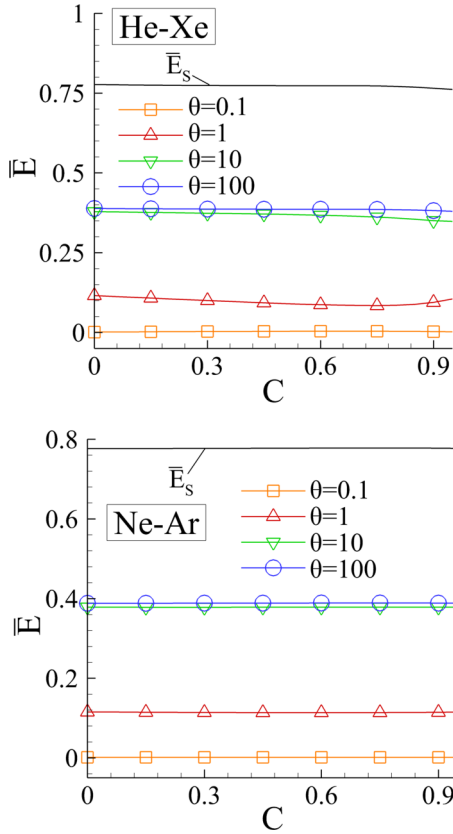


FIG. 11. Normalized cycle-average pumping power \bar{E}/dx of He-Xe and Ne-Ar in terms of C for $\delta = 1$ and $\theta = [0.1, 1, 10, 10^2]$ (\bar{E}_s is the steady-state pumping power).

The time-dependent pumping power $\tilde{E}(t)$ of the binary gas mixture, defined by Eq. (26) may be readily computed. The corresponding results are not presented here because the dependency of the mixture pumping power on the flow parameters is similar to the one observed in oscillatory single gas flow [9,11], i.e., as θ is decreased its amplitude is decreased and its phase angle lag is increased. Furthermore, the effect of the molar fraction C on the amplitude and phase angle of the mixture pumping power is very small.

Obviously, the pumping power has two peaks within each oscillatory cycle because it consists of the product of the oscillatory flow rate times the oscillatory pressure gradient and its integral over one cycle is not zero in order to drive the mixture flow, although the oscillatory net flow is zero. Therefore, by integrating $\tilde{E}(t)$ over one cycle, according to Eq. (27), the average pumping power is obtained. In Fig. 11 the normalized cycle-average pumping power \bar{E}/dx for the binary gas mixtures of He-Xe and Ne-Ar in terms of C is plotted for various values of $\theta = [0.1, 1, 10, 10^2]$ and the typical value of $\delta = 1$. The corresponding steady-state pumping power \bar{E}_s of the binary gas mixture flow of He-Xe and Ne-Ar are also plotted for comparison purposes. In general, as θ is decreased the cycle-average pumping power is decreased, which is expected since as the oscillation frequency is increased the flow rate amplitude is decreased. At large values of the oscillation parameter ($\theta \geq 10$), as the flow becomes stationary the cycle-average pumping power becomes half of

the corresponding steady-state one. The same trend has been observed in oscillatory single gas flows [9,11]. Furthermore, the effect of the molar fraction on the cycle-average pumping powers of He-Xe and Ne-Ar is very weak.

V. CONCLUDING REMARKS

The rarefied oscillatory pressure-driven fully developed isothermal binary gas mixture flow between parallel plates is computationally investigated in terms of the mixture molar fraction $C \in [0, 1]$ and the molecular mass ratio m_2/m_1 of the heavy over the light species, in a wide range of the gas rarefaction parameter δ and oscillation parameter θ , which are inversely proportional to the Knudsen number and the oscillation frequency respectively. Modeling is based on the McCormack kinetic model equation, subject to diffuse boundary conditions. The computed output quantities are in dimensionless form and include macroscopic quantities of theoretical and technological importance. More specifically, the amplitude and phase angle of the velocity distributions and flow rates of the two species, as well as of the flow rate and wall shear stress of the mixture are reported. In addition the time evolution of the mixture flow rate and the pumping power, as well as the cycle-average pumping power are provided. The results refer to the binary gas mixtures of He-Xe and Ne-Ar, while corresponding results of other mixtures are available upon request. The numerical work has been successfully validated in various ways, including grid refinement, fulfillment of the derived force balance benchmark expression and the analytical solution as $\theta \rightarrow 0$, as well as with systematic comparisons with corresponding works, available in the literature, at limiting conditions, such as steady-state binary gas flow as $\theta \rightarrow \infty$ [49] and oscillatory single gas flow when $C = 0$ or $m_1/m_2 = 1$ [9].

The flow rate, wall shear stress, and pumping power of the oscillatory binary gas mixture flow have qualitative resemblance with the corresponding ones in oscillatory single gas flow, in terms of δ and θ , but there are quantitative deviations particularly in the flow rates depending on C and m_2/m_1 . As in the case of single gases, as θ decreases (oscillation frequency increases), the amplitude of all quantities decreases and their phase angle increases. Also, inertia effects attenuate as the flow becomes more rarefied. The effect of the mixture components and its molar fraction is very important on the velocities and the corresponding flow rates of the species of the mixture, as well as on the ratio of their flow rate amplitudes.

Concerning the mixture quantities, it has been found that as m_2/m_1 is increased, the mixture flow rate amplitude is larger and the phase angle is smaller than the corresponding ones of the single gas. The variation with respect to C is nonmonotonic, taking the maximum and minimum values for the amplitude and the phase angle respectively at intermediate values of the molar fraction. The variation of the flow rate amplitude and the phase angle is more significant at small and large frequencies respectively. The time evolution of the mixture flow rate is in phase with the oscillatory pressure gradient when $\delta \ll \theta$ and completely out of phase when $\theta \ll \delta$. On the contrary, it has been found that the mixture wall shear stress and pumping power depend very weakly on C and m_2/m_1 in the whole range of δ and θ .

Concerning the species quantities and starting with the velocity distributions, it has been found that as the oscillation frequency is increased, although the velocity amplitudes of both species are decreased, the relative difference between the velocity amplitudes of the light and heavy species is increased. This behavior is observed at small δ and it becomes more pronounced as δ is increased, which is not expected, since as it is well-known gas separation effects are decreased as the flow becomes less rarefied and is dominated by intermolecular collisions. In parallel, the velocity phase angles of both species are increased, without observing a specific pattern with regard to their phase angle difference. Obviously, a similar behavior has been observed in the corresponding flow rates, which has been systematically investigated mainly in terms of the ratio of the flow rate amplitude of the light over the heavy species. As this ratio is increased gas separation is enlarged. In small oscillation frequencies (large θ), the variation of the ratio of the flow rate amplitude is the expected one, i.e., it is decreased as the flow becomes less rarefied. However, at moderate and high oscillation frequencies the behavior is reversed and the ratio of the flow rate amplitude is increased as the flow becomes less rarefied. It has been found that as θ decreases, the flow rate amplitude of the heavy species decreases much more significantly than of the light one and therefore, the ratio of the flow rate amplitude of the light over the heavy species is increased. This behavior, which is confirmed by the analytical solution at the high-frequency oscillation limit, is due to inertia effects, which are increased with the oscillation frequency, and they influence the velocity (and flow rate) amplitude of the heavy species much more than of the light one. This effect is further amplified as decreases, the flow rate amplitude of the heavy species decreases much more significantly than of the light one and therefore, the ratio of the flow rate amplitude of the light over the heavy species is increased. This behavior, which is confirmed by the analytical solution at the high-frequency oscillation limit, is due to inertia effects, which are increased with the oscillation frequency, and they influence the velocity (and flow rate) amplitude of the heavy species much more than of the light one. This effect is further amplified as δ is increased and the flow becomes less rarefied, overcoming diffusion effects due to intermolecular collisions, provided that θ is sufficiently small. This behavior depends weakly on C but very strongly on m_2/m_1 . It has been confirmed, both analytically and computationally, that at high frequencies the flow rate amplitude ratio of the light over the heavy species, independent of δ , tends to the molecular mass ratio of the heavy over the light species m_2/m_1 . In addition it has been physically explained and computationally prescribed that as the molecular mass of the gas species is increased, the velocity overshooting effect, well known in oscillatory flows, occurs in a thinner zone close to the wall and becomes more pronounced. Furthermore, it is worthwhile to note that the phase angle lag of the velocity and the flow rate of the heavy species are always larger than the corresponding ones of the light one.

It has been demonstrated that in oscillatory mixture flows, the difference between the velocities (and flow rates) of the light and heavy species, resulting to gas separation, may be increased as the gas rarefaction is reduced, provided that the

flow is subject to adequate high oscillation frequency. This is not the case in steady-state flow, where gas separation phenomena are diminished as the flow becomes less rarefied and tends to be in the hydrodynamic regime. However, oscillatory flows are in the hydrodynamic regime, only when the flow becomes less rarefied and oscillates at low frequencies and therefore in adequately high oscillatory flows, gas separation remains present in the whole range of gas rarefaction.

The present results may be useful in the design of various technological devices operating at moderate and high frequencies in the whole range of gas rarefaction, applicable in various technological fields. In addition to the McCormack model, BGK-type binary gas mixture models [69,73] may also be implemented.

However, since in oscillatory flow the net flow rate of each species is zero, it may be useful to point out that in the case of real gas separator apparatus, gas separation will be enhanced compared to the stationary flow, only if the reverse part of the oscillatory flow is significantly reduced or even completely eliminated compared to the forward part. This may be achieved by using a reciprocating pump or a check valve limiting the reverse flow. Another option is the implementation of a tapered channel to create a nonzero flow rate in the diverging direction of the channel, by exploiting the so-called diode effect [74]. More complex designs may also be considered by adjusting the channel length to be shorter than the tidal (gas) displacement of the light species and longer than the one of the heavy species. This way more particles of the light species compared to the heavy one will reach the downstream vessel, which should be accordingly evacuated, every half a cycle, to significantly reduce the reverse flow. All these are preliminary concepts explaining how the present results may be used in the design of oscillatory type gas separators even if the actual flow conditions are different than the ones assumed in the present flow configuration.

ACKNOWLEDGMENTS

This work has been carried out within the framework of the EUROfusion Consortium and has received funding from the Euratom research and training program 2014-2018 and 2019-2020 under Grant Agreement No. 633053. The views and opinions expressed herein do not necessarily reflect those of the European Commission. This computational work has been performed in the GRNET HPC facility - ARIS.

APPENDIX: THE LINEARIZED MCCORMACK COLLISION TERM

The linearized McCormack collision term in Eq. (38) for fully developed flow between parallel plates may be written as [49]

$$\begin{aligned}
 L_{\alpha\beta}h_a = & -\gamma_a h_a + 2\sqrt{\frac{m_a}{m}} [\gamma_{\alpha\beta} u_a - v_{\alpha\beta}^{(1)}(u_a - u_\beta) \\
 & - \frac{1}{2} v_{\alpha\beta}^{(2)} \left(q_a - \frac{m_a}{m_\beta} q_\beta \right)] c_{ax} \\
 & + 4 [(\gamma_{\alpha\beta} - v_{\alpha\beta}^{(3)}) \Pi_a + v_{\alpha\beta}^{(4)} \Pi_\beta] c_{ax} c_{ay}
 \end{aligned}$$

$$\begin{aligned}
 & + \frac{4}{5} \sqrt{\frac{m_a}{m}} \left[(\gamma_{\alpha\beta} - v_{\alpha\beta}^{(5)}) q_a + v_{\alpha\beta}^{(6)} \sqrt{\frac{m_\beta}{m_\alpha}} q_\beta \right. \\
 & \left. - \frac{5}{4} v_{\alpha\beta}^{(2)} (u_a - u_\beta) \right] c_{ax} \left(c_a^2 - \frac{5}{2} \right), \quad (\text{A1})
 \end{aligned}$$

with $\alpha = 1, 2, \beta \neq \alpha$. The collision frequencies $\gamma_a = \gamma_{aa} + \gamma_{\alpha\beta}$ are expressed as

$$\gamma_\alpha = \frac{S_a S_\beta - v_{\alpha\beta}^{(4)} v_{\beta\alpha}^{(4)}}{S_\beta + v_{\alpha\beta}^{(4)}}, \quad (\text{A2})$$

where $S_a = v_{aa}^{(3)} - v_{aa}^{(4)} + v_{a\beta}^{(3)}$ with $\alpha = 1, 2, \beta \neq \alpha$. The quantities $v_{\alpha\beta}^{(1-6)}$ are given by

$$v_{\alpha\beta}^{(1)} = \frac{16}{3} \frac{m_{\alpha\beta}}{m_a} n_\beta \Omega_{\alpha\beta}^{11}, \quad (\text{A3})$$

$$v_{\alpha\beta}^{(2)} = \frac{64}{15} \left(\frac{m_{\alpha\beta}}{m_a} \right)^2 n_\beta \left(\Omega_{\alpha\beta}^{12} - \frac{5}{2} \Omega_{\alpha\beta}^{11} \right), \quad (\text{A4})$$

$$v_{\alpha\beta}^{(3)} = \frac{16}{5} \frac{m_{\alpha\beta}^2}{m_a m_\beta} n_\beta \left(\frac{10}{3} \Omega_{\alpha\beta}^{11} + \frac{m_\beta}{m_a} \Omega_{\alpha\beta}^{22} \right), \quad (\text{A5})$$

$$v_{\alpha\beta}^{(4)} = \frac{16}{5} \frac{m_{\alpha\beta}^2}{m_a m_\beta} n_\beta \left(\frac{10}{3} \Omega_{\alpha\beta}^{11} - \Omega_{\alpha\beta}^{22} \right), \quad (\text{A6})$$

$$\begin{aligned}
 v_{\alpha\beta}^{(5)} = & \frac{64}{15} \left(\frac{m_{\alpha\beta}}{m_\alpha} \right)^3 \frac{m_\alpha}{m_\beta} n_\beta \left[\Omega_{\alpha\beta}^{22} + \left(\frac{15}{4} \frac{m_\alpha}{m_\beta} + \frac{25}{8} \frac{m_\beta}{m_\alpha} \right) \Omega_{\alpha\beta}^{11} \right. \\
 & \left. - \frac{1}{2} \frac{m_\beta}{m_\alpha} (5 \Omega_{\alpha\beta}^{12} - \Omega_{\alpha\beta}^{13}) \right], \quad (\text{A7})
 \end{aligned}$$

$$\begin{aligned}
 v_{\alpha\beta}^{(6)} = & \frac{64}{15} \left(\frac{m_{\alpha\beta}}{m_\alpha} \right)^3 \left(\frac{m_\alpha}{m_\beta} \right)^{3/2} n_\beta \left(-\Omega_{\alpha\beta}^{22} + \frac{55}{8} \Omega_{\alpha\beta}^{11} \right. \\
 & \left. - \frac{5}{2} \Omega_{\alpha\beta}^{12} + \frac{1}{2} \Omega_{\alpha\beta}^{13} \right), \quad (\text{A8})
 \end{aligned}$$

and

$$m_{\alpha\beta} = \frac{m_a m_\beta}{(m_a + m_\beta)}. \quad (\text{A9})$$

The Chapman-Cowling integrals $\Omega_{\alpha\beta}^{(ij)}$ for the rigid sphere interaction are written as

$$\Omega_{\alpha\beta}^{(ij)} = \frac{(j+1)!}{8} \left[1 - \frac{1+(-1)^i}{2(i+1)} \right] \left(\frac{\pi K T}{2 m_{\alpha\beta}} \right)^{(1/2)} (d_a + d_\beta)^2, \quad (\text{A10})$$

where $d_a, a = 1, 2$ is the diameter of the molecule of each species.

-
- [1] L. E. Kinsler, A. R. Frey, A. B. Coppens, and J. V. Sanders, *Fundamentals of Acoustics* (Wiley-VCH, New York, 1999), p. 560.
- [2] P. Cheng and T. S. Zhao, Heat transfer in oscillatory flows, *Ann. Rev. Heat Transf.* **9**, 359 (1998).
- [3] M. Zamir, *The Physics of Pulsatile Flow* (Springer New York, New York, 2000).
- [4] N. G. Hadjiconstantinou and O. Simek, Constant-wall-temperature Nusselt number in micro and nano-channels, *J. Heat Transf.* **124**, 356 (2002).
- [5] F. Sharipov and D. Kalempa, Oscillatory Couette flow at arbitrary oscillation frequency over the whole range of the Knudsen number, *Microfluid. Nanofluid.* **4**, 363 (2008).
- [6] D. Kalempa and F. Sharipov, Sound propagation through a rarefied gas confined between source and receptor at arbitrary Knudsen number and sound frequency, *Phys. Fluids* **21**, 103601 (2009).
- [7] L. Desvillettes and S. Lorenzani, Sound wave resonances in micro-electro-mechanical systems devices vibrating at high frequencies according to the kinetic theory of gases, *Phys. Fluids* **24**, 092001 (2012).
- [8] P. Wang, L. Zhu, W. Su, L. Wu, and Y. Zhang, Nonlinear oscillatory rarefied gas flow inside a rectangular cavity, *Phys. Rev. E* **97**, 043103 (2018).
- [9] A. Tsimpoukakis and D. Valougeorgis, Pulsatile pressure driven rarefied gas flow in long rectangular ducts, *Phys. Fluids* **30**, 047104 (2018).
- [10] A. Tsimpoukakis and D. Valougeorgis, Rarefied isothermal gas flow in a long circular tube due to oscillating pressure gradient, *Microfluid. Nanofluid.* **22**, 5 (2018).
- [11] A. Tsimpoukakis, N. Vasileiadis, G. Tatsios, and D. Valougeorgis, Nonlinear oscillatory fully-developed rarefied gas flow in plane geometry, *Phys. Fluids* **31**, 067108 (2019).
- [12] F. Sharipov, *Rarefied Gas Dynamics* (Wiley-VCH Verlag, Weinheim, Germany, 2016).
- [13] G. A. Bird, *Molecular Gas Dynamics and the Direct Simulation of Gas Flows* (Clarendon Press, Oxford, 1994).
- [14] G. H. Tang, X. J. Gu, R. W. Barber, D. R. Emerson, and Y. H. Zhang, Lattice Boltzmann simulation of nonequilibrium effects in oscillatory gas flow, *Phys. Rev. E* **78**, 026706 (2008).
- [15] P. Gospodinov, V. Roussinov, and S. Stefanov, Nonisothermal oscillatory cylindrical Couette gas flow in the slip regime: A computational study, *Eur. J. Mech. B* **33**, 14 (2012).
- [16] Y. Shi, Y. W. Yap, and J. E. Sader, Lattice Boltzmann method for linear oscillatory noncontinuum flows, *Phys. Rev. E* **89**, 033305 (2014).
- [17] L. Wu, Sound propagation through a rarefied gas in rectangular channels, *Phys. Rev. E* **94**, 053110 (2016).
- [18] K. Aoki, S. Kosuge, T. Fujiwara, and T. Goudon, Unsteady motion of a slightly rarefied gas caused by a plate oscillating in its normal direction, *Phys. Rev. Fluids* **2**, 013402 (2017).
- [19] Y. Ben-Ami and A. Manela, Nonlinear thermal effects in unsteady shear flows of a rarefied gas, *Phys. Rev. E* **98**, 033121 (2018).
- [20] Y. Ben-Ami and A. Manela, The sound of a pulsating sphere in a rarefied gas: Continuum breakdown at short length and time scales, *J. Fluid Mech.* **871**, 668 (2019).
- [21] T. Veijola, Gas damping in vibrating MEMS structures, in *Micro and Nano Technologies*, edited by M. Tilli, T. Motooka, V.-M. Airaksinen, S. Franssila, M. Paulasto-Krckel, and V. Lindroos (William Andrew Publishing, Boston, 2010), pp. 259–279.

- [22] Y. Ben Ami and A. Manela, Acoustic field of a pulsating cylinder in a rarefied gas: Thermoviscous and curvature effects, *Phys. Rev. Fluids* **2**, 093401 (2017).
- [23] A. Frezzotti, G. P. Ghiroldi, and L. Gibelli, Direct solution of the Boltzmann equation for a binary mixture on GPUs, in *27th International Symposium on Rarefied Gas Dynamics*, edited by D. A. Levin, I. J. Wysong and A. L. Garcia, AIP Conf. Proc. No. 1333 (American Institute of Physics, New York, 2011), pp. 884–889.
- [24] M. Bisi and S. Lorenzani, Damping forces exerted by rarefied gas mixtures in micro-electro-mechanical system devices vibrating at high frequencies, *Interfacial Phenomena Heat Transfer* **2**, 253 (2014).
- [25] M. Bisi and S. Lorenzani, High-frequency sound wave propagation in binary gas mixtures flowing through microchannels, *Phys. Fluids* **28**, 052003 (2016).
- [26] D. Kalempa and F. Sharipov, Sound propagation through a binary mixture of rarefied gases at arbitrary sound frequency, *Eur. J. Mech. B* **57**, 50 (2016).
- [27] D. Kalempa, F. Sharipov, and J. C. Silva, Sound waves in gaseous mixtures induced by vibro-thermal excitation at arbitrary rarefaction and sound frequency, *Vacuum* **159**, 82 (2019).
- [28] S. Lorenzani, Kinetic modeling for the time-dependent behavior of binary gas mixtures, in *31st International Symposium of Rarefied Gas Dynamics: RGD31*, edited by Y. Zhang, D. R. Emerson, D. Lockerby, and L. Wu, AIP Conf. Proc. No. 2132 (AIP, New York, 2019), p. 130006.
- [29] P. L. Bhatnagar, E. P. Gross, and M. Krook, A model for collision processes in gases. I. Small amplitude processes in charged and neutral one-component systems, *Phys. Rev.* **94**, 511 (1954).
- [30] F. J. McCormack, Construction of linearized kinetic models for gaseous mixtures and molecular gases, *Phys. Fluids* **16**, 2095 (1973).
- [31] S. Colin, C. Aubert, and R. Caen, Unsteady gaseous flows in rectangular microchannels: Frequency response of one or two pneumatic lines connected in series, *Eur. J. Mech. B* **17**, 79 (1998).
- [32] R. A. Abreu, Causes of anomalous solid formation in the exhaust systems of low-pressure chemical vapor deposition and plasma enhanced chemical vapor deposition semiconductor processes, *J. Vacuum Sci. Tech. B* **12**, 2763 (1994).
- [33] K. Jousten, Applications and scope of vacuum technology, in *Handbook of Vacuum Technology*, edited by K. Jousten (Wiley-VCH Verlag, Weinheim, Germany, 2016), pp. 518–520.
- [34] S. Colin, Rarefaction and compressibility effects on steady and transient gas flows in microchannels, *Microfluid. Nanofluid.* **1**, 268 (2005).
- [35] S. Chakraborty and A. P. S. Bhalla, Controlling microchannel gas flow rates through time-modulated pressure pulsation, *J. Appl. Phys.* **102**, 114910 (2007).
- [36] M. Nabavi and L. Mongeau, Numerical analysis of high frequency pulsating flows through a diffuser-nozzle element in valveless acoustic micropumps, *Microfluid. Nanofluid.* **7**, 669 (2009).
- [37] S. Wang, A. Batikh, L. Baldas, A. Kourta, N. Mazellier, S. Colin, and S. Orieux, On the modeling of the switching mechanisms of a Coanda fluidic oscillator, *Sensors Actuators A: Phys.* **299**, 111618 (2019).
- [38] J. S. Stecki and D. C. Davis, Fluid transmission lines-distributed parameter models part I: A review of the state of the art, *Proc. Inst. Mechanical Eng. A* **200**, 215 (1986).
- [39] I. J. Karassik, J. P. Messina, P. Cooper, and C. C. Heald, *Pump Handbook* (McGraw-Hill, New York, 2000).
- [40] J. B. Heywood, *Internal Combustion Engine Fundamentals* (McGraw-Hill, New York, 1988).
- [41] K. B. Heraty, J. G. Laffey, and N. J. Quinlan, Fluid dynamics of gas exchange in high-frequency oscillatory ventilation: In vitro investigations in idealized and anatomically realistic airway bifurcation models, *Ann. Biomed. Eng.* **36**, 1856 (2008).
- [42] U. H. Kurzweg, Enhanced heat conduction in oscillating viscous flows within parallel-plate channels, *J. Fluid Mech.* **156**, 291 (1985).
- [43] A. M. Thomas, Unusual effects of oscillating flows in an annulus on mass transfer and separation, *Adv. Space Res.* **32**, 279 (2003).
- [44] Z. Yu, X. Mao, and A. J. Jaworski, Experimental study of heat transfer in oscillatory gas flow inside a parallel-plate channel with imposed axial temperature gradient, *Int. J. Heat Mass Transf.* **77**, 1023 (2014).
- [45] A. Hacıoglu and R. Narayanan, Oscillating flow and separation of species in rectangular channels, *Phys. Fluids* **28**, 073602 (2016).
- [46] G. J. Brereton and S. M. Jalil, Diffusive heat and mass transfer in oscillatory pipe flow, *Phys. Fluids* **29**, 073601 (2017).
- [47] S. M. Jalil, Experimental and numerical investigation of axial heat transfer enhancement by oscillatory flows, *Int. J. Therm. Sci.* **137**, 352 (2019).
- [48] F. Sharipov and D. Kalempa, Gaseous mixture flow through a long tube at arbitrary Knudsen numbers, *J. Vacuum Sci. Tech. A* **20**, 814 (2002).
- [49] S. Naris, D. Valougeorgis, D. Kalempa, and F. Sharipov, Gaseous mixture flow between two parallel plates in the whole range of the gas rarefaction, *Physica A* **336**, 294 (2004).
- [50] S. Naris, D. Valougeorgis, D. Kalempa, and F. Sharipov, Flow of gaseous mixtures through rectangular microchannels driven by pressure, temperature, and concentration gradients, *Phys. Fluids* **17**, 100607 (2005).
- [51] R. D. M. Garcia and C. E. Siewert, Channel flow of a binary mixture of rigid spheres described by the linearized Boltzmann equation and driven by temperature, pressure, and concentration gradients, *SIAM J. Appl. Math.* **67**, 1041 (2007).
- [52] L. Szalmas, J. Pitakarnnop, S. Geoffroy, S. Colin, and D. Valougeorgis, Comparative study between computational and experimental results for binary rarefied gas flows through long microchannels, *Microfluid. Nanofluid.* **9**, 1103 (2010).
- [53] L. Szalmas, Isothermal flows of rarefied ternary gas mixtures in long tubes, *Microfluid. Nanofluid.* **17**, 1095 (2014).
- [54] F. Sharipov and D. Kalempa, Separation phenomena for gaseous mixture flowing through a long tube into vacuum, *Phys. Fluids* **17**, 127102 (2005).
- [55] D. Kalempa and F. Sharipov, Flows of rarefied gaseous mixtures with a low mole fraction. Separation phenomenon, *Eur. J. Mech. B* **30**, 466 (2011).
- [56] M. Vargas, S. Naris, D. Valougeorgis, S. Pantazis, and K. Jousten, Time-dependent rarefied gas flow of single gases and binary gas mixtures into vacuum, *Vacuum* **109**, 385 (2014).

- [57] D. Valougeorgis, M. Vargas, and S. Naris, Analysis of gas separation, conductance and equivalent single gas approach for binary gas mixture flow expansion through tubes of various lengths into vacuum, *Vacuum* **128**, 1 (2016).
- [58] S. Nakaye, H. Sugimoto, N. K. Gupta, and Y. B. Gianchandani, Thermally enhanced membrane gas separation, *Eur. J. Mech. B* **49**, 36 (2015).
- [59] S. Nakaye and H. Sugimoto, Demonstration of a gas separator composed of Knudsen pumps, *Vacuum* **125**, 154 (2016).
- [60] Y. Qin and Y. B. Gianchandani, A fully electronic micro-fabricated gas chromatograph with complementary capacitive detectors for indoor pollutants, *Microsyst. Nanoeng.* **2**, 15049 (2016).
- [61] S. Takata, H. Sugimoto, and S. Kosuge, Gas separation by means of the Knudsen compressor, *Eur. J. Mech. B* **26**, 155 (2007).
- [62] V. V. Kosyanchuk, A. N. Yakunchikov, I. A. Bryukhanov, and S. A. Konakov, Numerical simulation of novel gas separation effect in microchannel with a series of oscillating barriers, *Microfluid. Nanofluid.* **21**, 116 (2017).
- [63] V. V. Kosyanchuk and A. N. Yakunchikov, Simulation of gas separation effect in microchannel with moving walls, *Microfluid. Nanofluid.* **22**, 60 (2018).
- [64] S. Meskos, S. Stefanov, and D. Valougeorgis, Gas mixing and final mixture composition control in simple geometry micro-mixers via DSMC analysis, *Micromachines* **10**, 178 (2019).
- [65] T. Baier and S. Hardt, Gas separation in a Knudsen pump inspired by a Crookes radiometer, *Microfluid. Nanofluid.* **24**, 41 (2020).
- [66] R. L. Panton, *Incompressible Flow* (John Wiley & Sons, Hoboken, NJ, 2013).
- [67] M. J. Jaeger, T. Soepardi, A. Maddahian, and U. Kurzweg, Diffusional separation of gases and solutes in oscillatory flow, *Separation Sci. Tech.* **26**, 503 (1991).
- [68] F. Sharipov, Ab initio simulation of gaseous mixture flow through an orifice, *Vacuum* **143**, 106 (2017).
- [69] S. Lorenzani, A microchannel flow application of a linearized kinetic Bhatnagar-Gross-Krook-type model for inert gas mixtures with general intermolecular forces, *Phys. Fluids* **31**, 072001 (2019).
- [70] F. Sharipov, L. M. Gramani Cumin, and D. Kalempa, Plane Couette flow of binary gaseous mixture in the whole range of the Knudsen number, *Eur. J. Mech. B* **23**, 899 (2004).
- [71] J. Kestin, K. Knierim, E. A. Mason, B. Najafi, S. T. Ro, and M. Waldman, Equilibrium and transport properties of the noble gases and their mixtures at low density, *J. Phys. Chem. Ref. Data* **13**, 229 (1984).
- [72] D. Valougeorgis, The friction factor of a rarefied gas flow in a circular tube, *Phys. Fluids* **19**, 091702 (2007).
- [73] P. Andries, K. Aoki, and B. Perthame, A consistent BGK-type model for gas mixtures, *J. Stat. Phys.* **106**, 993 (2002).
- [74] I. Graur, J. G. Méolans, P. Perrier, J. Thöming, and T. Veltzke, A physical explanation of the gas flow diode effect, *Microfluid. Nanofluid.* **20**, 145 (2016).